

**REPORT DOCUMENTATION PAGE**

AFRL-SR-BL-TR-02-

Public reporting burden for this collection of information is estimated to average 1 hour per response, including the time for reviewing instruction the collection of information. Send comments regarding this burden estimate or any other aspect of this collection of information, including Operations and Reports, 1215 Jefferson Davis Highway, Suite 1204, Arlington, VA 22202-4302, and to the Office of Management and Budget.

and reviewing  
or Information

0260

<b>1. AGENCY USE ONLY (Leave blank)</b>		<b>2. REPORT DATE</b> FINAL	<b>3. RL</b> 15 Nov 1998 - 14 Nov 2001
<b>4. TITLE AND SUBTITLE</b> Hypersonic Maneuvering Vehicles Simulations Using Real-Gas, Unstructured Navier-Stokes Software		<b>5. FUNDING NUMBERS</b> F49620-99-C-0001	
<b>6. AUTHOR(S)</b> William D. McGrory			
<b>7. PERFORMING ORGANIZATION NAME(S) AND ADDRESS(ES)</b> AeroSoft, Inc. 1872 Pratt Drive, Suite 1275 Blacksburg, VA 24060-6363		<b>8. PERFORMING ORGANIZATION REPORT NUMBER</b>	
<b>9. SPONSORING/MONITORING AGENCY NAME(S) AND ADDRESS(ES)</b> AFOSR 801 N. RANDOLPH STREET, ROOM 732 ARLINGTON, VA 22203-1977		<b>10. SPONSORING/MONITORING AGENCY REPORT NUMBER</b>  F49620-99-C-0001	
<b>11. SUPPLEMENTARY NOTES</b>			
<b>12a. DISTRIBUTION AVAILABILITY STATEMENT</b> APPROVED FOR PUBLIC RELEASE, DISTRIBUTION UNLIMITED		<p align="center">AIR FORCE OFFICE OF SCIENTIFIC RESEARCH NOTICE OF TRANSMISSION THIS TECHNICAL REPORT HAS BEEN REVIEWED AND IS APPROVED FOR PUBLIC RELEASE IN ACCORDANCE WITH FAR PART 101-11.6 LAW AFR 190-12. DISTRIBUTION IS UNLIMITED</p>	
<b>13. ABSTRACT (Maximum 200 words)</b> Hypersonic vehicles are becoming more of a reality with the current level of technology. Concept vehicles are now being made in order to test the most recent advances in hypersonic technology. Along with models for flight testing, CFD has become an important role in the development of modern hypersonic vehicles. The technology in CFD is making more complex configurations and flow-fields available for simulation. One of the advances in CFD that is making this possible is unstructured grid generation and flow solvers.			
<b>14. SUBJECT TERMS</b>		<b>15. NUMBER OF PAGES</b> 49	
		<b>16. PRICE CODE</b>	
<b>17. SECURITY CLASSIFICATION OF REPORT</b>	<b>18. SECURITY CLASSIFICATION OF THIS PAGE</b>	<b>19. SECURITY CLASSIFICATION OF ABSTRACT</b>	<b>20. LIMITATION OF ABSTRACT</b>

20020305 116

**FINAL REPORT**

**CONTRACT No. F49620-99-C-0001**

**“HYPERSONIC MANEUVERING VEHICLE SIMULATIONS  
USING REAL-GAS, UNSTRUCTURED NAVIER-STOKES  
SOFTWARE”**

*William D. McGrory, Principal Investigator*  
AeroSoft, Inc.  
1872 Pratt Drive, Suite 1275  
Blacksburg, Virginia 24060-6363  
(540) 557-1900  
(540) 557-1919 (FAX)  
<http://www.aerosft.com>

# Table of Contents

0.2	Introduction . . . . .	1
0.3	Objectives . . . . .	3
0.4	Work Plan . . . . .	4
0.5	Preliminary Simulations . . . . .	6
0.5.1	Case 1: 3-D, Inviscid, Perfect Gas . . . . .	6
0.5.2	Case 2: 2-D, Viscous, Perfect Gas . . . . .	7
0.5.3	Step 3: 3-D, Viscous, Perfect Gas . . . . .	8
0.5.4	Step 4: 2-D, Viscous, Chemistry . . . . .	8
0.6	Final Simulations . . . . .	10
0.6.1	Grid Generation & Selection . . . . .	10
0.6.2	Engine Off Simulation . . . . .	14
0.6.3	Engine On Simulation . . . . .	36
0.6.4	Time Accurate Simulation . . . . .	44
0.7	Conclusions . . . . .	47

## 0.2 Introduction

Hypersonic vehicles are becoming more of a reality with the current level of technology. Concept vehicles are now being made in order to test the most recent advances in hypersonic technology. Along with models for flight testing, CFD has become an important role in the development of modern hypersonic vehicles. The technology in CFD is making more complex configurations and flow-fields available for simulation. One of the advances in CFD that is making this possible is unstructured grid generation and flow solvers.

AeroSoft has computed the flow-field around a hypersonic aerodynamic vehicle using current CFD technology. The simulation was performed at Mach 6 with a 0 and 2 degree angle of attack and included chemistry to

simulate the combustion of hydrogen in the scramjet. The aerodynamic flow-field was computed using *GUST*, AeroSoft's unstructured CFD software package. *GUST* consists of a flow solver, a post processor, and several support utilities. *GUST* also has an unstructured grid generator for both two and three-dimensional meshes. The grid generator will be referred to as *ASTET* throughout the remainder of this report.

*GUST* is capable of accurately simulating time-dependent problems whose domain can be described with multiple, non point-to-point connecting grids. Time-dependent problems can also be simulated where the boundaries of the grid move in relative motion. The unstructured code is optimized for vectorization on vector-based supercomputers and parallelization via domain decomposition on shared memory and distributed multiprocessor architectures such as Cray and Silicon Graphics supercomputers. The current capabilities of the unstructured flow solver are briefly summarized below.

### **Unstructured Fluid Dynamics Code (*GUST*) Capabilities**

- Solves integral form of the Reynolds Averaged Navier-Stokes equations
- Arbitrary cell types in any combination (e.g., tetrahedra, prisms, and hexahedra)
- Multi-zone/multi-partition parallel capabilities
- Linear (2nd-order accurate) reconstruction
- Finite-rate and equilibrium chemistry
- Vibrational non-equilibrium and equilibrium thermodynamics
- Space marching via domain decomposition and multi-zone.
- Utilizes the message passing interface (MPI) for a highly parallelized algorithm for distributed architectures.
- Implicit and explicit boundary conditions.
- One and two equation isotropic turbulence models.
- Graphical user interface for the input deck.

*ASTET* is AeroSoft's two-dimensional and three-dimensional unstructured grid generator based upon the advancing-front algorithm. An additional algorithm feature assures that the resulting mesh qualifies as a De-launey triangulation. Starting at the computational boundaries, the advancing-front algorithm introduces nodes and cells, one at a time, until the entire domain is discretized. For a viscous layer, prisms are used to discretize the boundary layer. Prisms are layered until either a set number of cells are reached or the cell size matches that of the overlaying tetrahedra grid. This algorithm benefits by generating the nodes and connectivity information simultaneously. In addition, the grid-point distribution and cell orientation are completely arbitrary making the generalized-discretization approach ideal for solution adaptation. The unstructured grid generators have their own graphical user interfaces which makes the grid generation process user friendly.

With the use of the *ASTET*, AeroSoft was able to generate a multi-zone viscous mesh about a generic hypersonic vehicle. With the mesh generated, AeroSoft was then able to simulate several hypersonic vehicle configurations using the *GUST* flow solver. Simulations included engine on and engine off constant flight configurations and a pull up maneuver.

### 0.3 Objectives

AeroSoft proposed to compute the flow-field around a hypersonic aerodynamic vehicle using unstructured CFD technology. The geometry of the hypersonic vehicle was given to AeroSoft in the form of an IGES file. A view of the vehicle is shown in Figure 11.

The simulation of the hypersonic vehicle was performed using AeroSoft's unstructured software package. This consisted of *GUST*, a CFD flow solver and *ASTET*, a grid generator. The capabilities of *GUST* and *ASTET* were demonstrated with the full simulation of the hypersonic vehicle.

The objectives for this work are three-fold. These are listed below in order that they were performed.

- Perform a complete nose-to-tail, three dimensional Navier-Stokes simulation about a realistic hypersonic vehicle. Air will flow through the vehicle's scramjet, but no combustion will take place (no fuel injection). Real gas effects will be modeled for the entire flowfield.

- Perform the objective above but with combustion, thus modeling the internal combustion and external exhaust plume.
- Perform a time accurate, engine-off pitch maneuver with the hypersonic vehicle. The maneuver will be a prescribed in-flight pull-up.

## 0.4 Work Plan

This section discusses the approach that AeroSoft took to accomplish the objectives. It did not seem wise to go straight to the three-dimensional engine off problem (first objective) without first investigating the problem itself. A full body, viscous real gas simulation is not trivial for the hypersonic vehicle of interest here. Determination of the grid resolution and quality were very important, as well as understanding the physics that the flow solver needed to model. AeroSoft therefore took a methodical approach to fulfilling the contract objectives.

In the first two objectives, AeroSoft was to perform two CFD calculations of the hypersonic vehicle at a prescribed flight condition. This flight condition is given in Table 1. The simulation included the modeling of turbulent flow about the entire vehicle, including the internal nozzle of the scramjet. The combustion of hydrogen was simulated with both engine on and engine off conditions.

In order to accomplish the first and second objectives, AeroSoft took a modular approach to the problem. By taking the hypersonic vehicle problem and breaking it down into less complex cases, AeroSoft was better able to understand both the physics and numerics of the complete simulation. This allowed for issues to be identified and dealt with one at a time. Each simplification focused on a particular aspect of the problem, giving insight and experience for when the full simulation was to be performed. AeroSoft divided the problem into four cases, after which the full simulation of the hypersonic vehicle was to be performed. These four cases are described next.

The first case in the hypersonic calculation was to perform an inviscid, perfect gas simulation about the complete three-dimensional vehicle. This allowed the inviscid effects of the vehicle to be studied and to verify the outer boundary of the mesh. Also with this case, the geometry was prepared for future grid generation.

After the first case was complete, a two-dimensional problem was made using the geometry along the symmetry plane. A viscous 2-D mesh was generated, and the effects of adding turbulence to the problem was studied. In this case, the flow was assumed to behave as a perfect gas.

For the third case, a three-dimensional calculation was performed on just the front half of the vehicle. A viscous grid was generated consisting of prisms and tetrahedras. The calculation was performed using a one-equation turbulence model with perfect gas chemistry.

In the fourth case, the scramjet was focused on. A new 2-D mesh was made to study just the scramjet region. A seven specie hydrogen-air chemistry model was used to simulate combustion in the engine chamber. The simulation was performed using a one-equation turbulence model in conjunction with finite rate chemistry.

With the four test cases complete, AeroSoft was then in a position to run the full simulation on the hypersonic vehicle. A full, three-dimensional viscous grid was generated about the hypersonic vehicle using knowledge that was gained from running the four test cases. The grid had eight zones, and consisted of hexahedras, prisms, and tetrahedras. With this mesh, both the engine on and engine off simulations were performed.

In the next section, each of the four steps mentioned above will be explained in more detail. Results from each computation will also be shown and discussed. The section after that presents the full simulation results, which fulfilled the contract objectives.

Table 1: Hyper-X Flow Conditions.

Free-stream Mach No., $M_{inf}$	6.0
Free-stream Velocity, $V_{inf}$	912.54 $m/s$
Temperature	57.59° $K$
Pressure	497.33 $N/m^2$
Reynolds number, $R_e$	$7.245 \times 10^6/m$
Mixture Density	0.0301 $kg/m^3$
angle of attack	0°, 2° degrees

## 0.5 Preliminary Simulations

The computations that were performed for the hypersonic vehicle utilized most of the features available in *GUST*. For example, the full Navier-Stokes equations were solved using turbulence models, chemistry models with up to seven species, frozen and finite rate chemistry, and Chimera grid techniques. Since the hypersonic vehicle simulations were numerically and physically complex, some preliminary computations were performed

The preliminary calculations were a simplification of the real problem. Four preliminary calculations were performed before starting the simulations as specified in the objectives. These preliminary computations gave valuable insight into the physics of the hypersonic vehicle problem. Numerical issues were also exposed that could be avoided for the full simulations.

The four preliminary calculations are discussed next. These calculations simplify the physical problem by assuming one or more of the following: two-dimensional flow instead of three-dimensional, inviscid flow instead of turbulence, and perfect gas instead of chemically reacting gas.

### 0.5.1 Case 1: 3-D, Inviscid, Perfect Gas

The first preliminary computation that was performed in the hypersonic vehicle calculation was an inviscid, perfect gas simulation about the three-dimensional vehicle. This calculation allowed the full configuration to be solved for, but with the inviscid and perfect gas assumption.

For this simulation, an unstructured mesh consisting of tetrahedras was generated using *ASTET*. The geometry of the hypersonic vehicle was given to *ASTET* in the form of an IGES file. *ASTET* imported the IGES file and converted the units to meters (the original data was in millimeters). The surfaces and curves were then set-up and trimmed for grid generation. A grid consisting of a single zone with 196,576 tetrahedra cells was made.

Figure 1 shows the pressure contours on the symmetry plane for this case. The shock that originates off the front of the vehicle is within the outer boundary of the grid domain. The outer limits on the grid are therefore sufficient for the flight condition tested. In this first test case, the flow is passing through the nozzle as if to simulate the engine off condition. The pressure in the flow-field is highest in the engine region due to flow compression.

A second figure shows the surface pressure contours near the scramjet inlet area (Figure 2). The grid for this problem was coarse, and was refined

for the full 3-D problem.

### 0.5.2 Case 2: 2-D, Viscous, Perfect Gas

The second preliminary case performed for the hypersonic vehicle solved the flow-field in two-dimensions. For this case, a viscous grid was generated using *ASTET*, and the Spalart-Allmaras turbulence model was used to model the turbulent flow. This case was performed in order to study both the numerical and physical aspects of the flow-field when using a turbulence model. In many problems, insight about running a 3-D problem can be gained by first simplifying the problem to two dimensions.

The grid was taken about the vehicle symmetry plane and included the flow through the scramjet. No chemical reactions were modeled in this case (case four contains chemistry). The Spalart-Allmaras one equation turbulence model was chosen due to its robustness over two-equation models. In CFD calculations involving one-equation turbulence models, the Spalart-Allmaras model has quickly become the model of choice. As the number of equations increase in a turbulence model, experience has shown that the difficulty in computing complex viscous problems increase. More attention and time must be given to two-equation models when performing CFD computations that involve large regions of separation, shocks, or strong expansions. The Spalart-Allmaras one equation model provides a good blend of model sophistication with numerical efficiency and robustness.

What was learned from this case was how to possibly run the 3-D problem for a viscous calculation. Unlike an inviscid computation, the viscous fluxes and turbulence model are much more sensitive to the initial conditions, especially inside the scramjet where the injection of hydrogen is to occur. A low Mach number (Mach 0.5 was chosen to initialize the flow in this problem) should be used to initialize the grid when starting the computation using the Spalart-Allmaras turbulence model. The case was ran with success, but due to the limitations of the grid generation process for viscous, 2-D geometries, the grid quality was not sufficient. Test case four deals with grid quality in more detail for the scramjet.

Figure 3 is a plot of contour lines for the turbulent viscosity. Aside from the boundary layer, most of the activity takes place around the nozzle inlet. Note that shocks and expansions tend to generate turbulent viscosity with one and two equation turbulence models, which can cause numerical instability if not limited.

### 0.5.3 Step 3: 3-D, Viscous, Perfect Gas

In the third preliminary computation, a three dimensional grid was generated for the front half of the hypersonic vehicle. The purpose of this case was two-fold. The first being to create a viscous 3-D grid using *ASTET*, and the second to run the hypersonic vehicle in 3-D using the Spalart-Allmaras turbulence model discussed in case two.

*ASTET* was used to generate the three dimensional viscous grid. The algorithm is based on the advancing layer method where the viscous layer, which is prism based, was generated first. The viscous layer was generated normal to the surface until either a specified number of layers were generated, or until selected tolerances were met. An example of one of the tolerances being met is when the cell size of the prism approached the size of the background grid. The tolerances are designed to give valid cells in the viscous layer, as well as to ensure a smooth blending from prisms to tetrahedras.

Only the front portion of the hypersonic vehicle was generated and used in this case. A single zone grid was attempted about the complete vehicle, but due to several singular points, the advancing layers algorithm failed. Therefore, the grid was broken up into zones. Due to the limitations of the grid generator, point-to-point zonal boundaries are not possible for viscous grids, so zones were generated which do not have cell to cell connectivity across zones. *GUST* has both chimera and non-point-to-point zonal boundary capabilities, which will be used for the full simulation using the generated zones.

The test case ran and showed that the grid for the viscous layer was adequate to resolve the boundary layer. The grid along the symmetry plane is shown in Figure 4. Note the smooth blending from the viscous layer (prisms) to the inviscid flow field (tetrahedras).

Several other plots showing pressure contours are given in Figures 5 and 6. These figures show the pressure on the vehicle surface and the symmetry plane respectively. The flow-field does not include the scramjet, and ends just before the tail fin starts.

### 0.5.4 Step 4: 2-D, Viscous, Chemistry

The fourth and final preliminary computation focused on the scramjet geometry and the simulation of hydrogen combustion. The case was ran in two dimensions, and consisted of only the internal flow through the scramjet.

Due to the simple geometry inside the scramjet and the flexibility of *GUST*, a structured grid was used for the computation. An unstructured viscous grid could have been generated using *ASTET* (which was done in case two), but the quality of the grid would not have been as good as the structured grid used here. While the generation of unstructured grids are fast compared to the structured grid generation process, the capabilities of unstructured viscous grid generation is not as advanced. In the future, the algorithms and software will be more advanced and good quality viscous grids will be more easily generated using unstructured grid generators. But for the present, the ability of *GUST* to use both structured and unstructured grids will be taken advantage of. Not only can *GUST* run on a structured grid, but *GUST* will allow the grid type to change from zone to zone, thus allowing both structured and unstructured grids to be used in the same problem.

Since no injection conditions were given to AeroSoft, this case allowed the conditions of hydrogen to be determined, which would then be used in the 3-D case. As a first attempt, the stoichiometric conditions for a hydrogen-air combustion were assumed to determine the density of each specie. The injection velocity was taken slightly above Mach one, and due to the low temperature of the free-stream flow, a high injection temperature was imposed ( $2000^{\circ}K$ ). With these conditions, combustion would occur, but due to the pressure of hydrogen coming into the flow, the throat of the nozzle became subsonic. Since a scramjet is to be simulated in this problem, the conditions were changed in order to maintain a supersonic flow throughout the scramjet. The density was therefore decreased while keeping the Mach number and temperature constant. The hydrogen was injected into the flow along the backward facing portion of the steps inside the nozzle. The direction angle of the hydrogen being injected was at zero degrees.

Several plots are presented for this case. The first plot (Figure 7), shows the Mach number contours inside the scramjet due to the combustion of hydrogen. The flow remains supersonic throughout the scramjet. Figure 8 and 9 show the mass fraction contours for hydrogen and water respectively. The combustion appears to be lean since very little hydrogen remains downstream of the injection.

## 0.6 Final Simulations

With the preliminary calculations performed, computations were then started that would accomplish the project objectives. The engine off simulation would be performed first, followed by the engine-on simulation. And last of all the prescribed flight maneuver would be done.

Before doing the CFD computations, a viscous grid for the complete hypersonic vehicle would need to be created. This was one of the more challenging aspects of the project due to the technology development in this area. A high quality unstructured viscous grid is difficult to attain for complex geometries such as the hypersonic vehicle. Because of this, three different grid generation software packages were looked at. These were GRIDGEN, ICEM CFD, and AeroSoft's unstructured grid generator *ASTET*.

A discussion on the grid generation process will be presented first. Following that will be the CFD simulations, which used the same grid for the engine on and engine off configurations, and a second grid for the prescribed flight maneuver.

### 0.6.1 Grid Generation & Selection

The work performed in this project has highlighted one problem area for unstructured, 3D Navier-Stokes simulations. This problem area lies with the grid quality and generation. In theory, an unstructured mesh gives greater flexibility in modeling complex geometries. For inviscid solutions, this has shown to be true over the past decade. With the additional requirement of resolving viscous flow features such as the boundary layer, problems quickly arise in unstructured grid generation. Unstructured grid generators have the ability to create viscous grids, but this added requirement adds complexity and time to the grid generation process. And the quality of an unstructured viscous grid is usually not as good as those of traditional structured grids.

The hypersonic vehicle that was used for the CFD computations is considered a complex geometry. It has multiple sharp edges and corners, as well as an internal duct used to model a scramjet. One of the more problematic aspects of the geometry was the existence of a singular point. The vertical fins joined the body of the vehicle in such a way that a singular point was formed.

The problem with the singular point lies mainly with viscous grid generation. The singular point joined multiple surfaces in which there was no

common normal vector. A view of the singular point is given in Figure 10. A normal vector is used to direct the growth of the viscous grid layer. The normal vector at the singular point is undefined, which results in a negative volume cell for one of the surfaces joining the singular point. Because of this, it is nearly impossible to generate a high quality viscous grid with point-to-point connectivity for this geometry.

*ASTET*, which is AeroSoft's unstructured grid generation code, was used for all the preliminary calculations. It was also the first choice in trying to generate a full viscous grid about the hypersonic vehicle. It uses the advancing front/hybrid hyperbolic method to generate the viscous layer. In short, *ASTET* first generates a surface triangular mesh. From the surface mesh, prisms are generated off of the surface normal to the body. The prism cells form layers around the body. These layers grow along with the cell size so as to blend with the outer tetrahedral cells, which make up the remainder of the mesh. In this way, a smooth, good quality viscous grid can be achieved. At its current state of development, *ASTET* is limited to single zone generation for hybrid viscous grids.

*ASTET* had several problems generating a single zone grid for the hypersonic geometry. The first problem arose with the singular point. This point in the geometry, as discussed above, caused negative volume cells which were not acceptable with the flow solver. And since *ASTET* was limited to single zone grids for viscous problems, this prevented a point-to-point single zone grid for the entire hypersonic vehicle.

The second problem area for *ASTET* was the internal duct region. The internal duct caused a problem with *ASTET* because of the relative size of the duct compared with the rest of the vehicle. *ASTET* has one set of size parameters for the viscous layer algorithm which were not the same for both the exterior surface and interior duct. This prevented the generation of a good quality viscous grid for both the internal duct and the external surfaces.

Because of these two factors, *ASTET* was unable to generate a single zone hybrid viscous grid around the entire hypersonic vehicle. AeroSoft then came up with a different approach to the grid generation that would circumvent the problems with *ASTET*. To get around the problem with the singular point, multiple zones were generated with non point-to-point connectivity. The front half of the vehicle (split at the singular point) was made into one zone, while the rear of the vehicle was broken into three zones. The three rear zones consisted of the top, side, and bottom of the vehicle rear. Again

each zone was broken around the singular point. The outline of the four zones are shown in Figure 11.

For the internal duct, another approach was taken. The internal duct would now be modeled with one or more zones. Since the internal duct has a simple geometry (converging diverging nozzle with a step), it would be easy to generate a structured (hexahedral) grid. Using GRIDGEN, a four zone structured viscous grid was generated and used to mesh the internal duct. AeroSoft added several dividers inside the duct to simulate partitions within the scramjet. A view of the duct is shown in Figure 12. In this picture, the solid surface corresponds to the internal duct geometry, while the external vehicle is shown as lines for clarity of the duct.

In summary, the viscous grid generated with *ASTET* and GRIDGEN consisted of eight zones. The grid had a total of 1,191,399 grid cells. Four of the zones were generated with *ASTET* and consisted of prisms and tetrahedra. The prisms were used in the viscous layer and the tetrahedra in the remainder of the flowfield. The zones generated from *ASTET* meshed up the majority of the flowfield (1,036,879 cells). The internal duct had a four zone grid consisting of hexahedras and was generated using GRIDGEN. A view of the grid is shown in Figure 13. In this view, a slice of the grid has been taken showing the internal duct and external surface mesh. The non point-to-point *ASTET* zonal boundary is also seen in the figure. A characteristic of *ASTET* is the smooth blending of the viscous prism layer to the tetrahedral cells.

Because of the need to use non point-to-point zonal boundaries to generate the hypersonic vehicle grid, the Chimera method was implemented into *GUST*. The Chimera algorithm is commonly used for overlapping grids, but in this case the technology was used to run the non point-to-point zonal boundary grids. This new feature of *GUST* made running the the hypersonic vehicle possible with the *ASTET* grid.

In a desire to eliminate the non point-to-point connectivity associated with the *ASTET* grid, other grid generation software packages were studied. AeroSoft looked at the commercial grid generation codes GRIDGEN and ICEM CFD. The GRIDGEN and ICEM CFD software packages have been in use for a long time, and represent some of the leading grid generation software available.

GRIDGEN uses a similar approach to *ASTET* for its unstructured grid generation. A surface grid is first constructed. The viscous layer is then marched off the surface. The remaining volume grid is then generated to

complete the grid generation process. After looking into the unstructured grid features of GRIDGEN, it was found that a good quality single zone grid was not possible using GRIDGEN. Like *ASTET*, the software did not support multiple zones with point-to-point connectivity.

At the time of testing, the tools offered by GRIDGEN for unstructured grid generation were lacking in capabilities when compared to its structured grid generator. On the positive side, GRIDGEN has the advantage of being a user friendly software with the potential of handling complex geometries like the hypersonic vehicle in the near future. To conclude, no unstructured grids were generated using GRIDGEN for the hypersonic vehicle.

ICEM CFD offers a grid generation software package with a different methodology than both GRIDGEN or *ASTET*. To generate an unstructured viscous grid with ICEM CFD, an inviscid grid must first be generated. Afterward, the viscous surfaces are specified, along with viscous grid parameters. The viscous layer is then added and meshed to the existing inviscid grid. An inviscid grid was generated for the hypersonic vehicle which consisted of 791,018 tetrahedral cells. But unfortunately, a good quality viscous grid was never generated with the software.

There are a lot of options available for the user in order to create a grid with ICEM. Though promising, the ICEM CFD software did not yield the desired grid with the time spent using the software. With more in-depth training on the software, it is possible that ICEM CFD would generate an acceptable grid for the hypersonic vehicle. Some drawbacks to the software were observed. The blending of viscous cells to the inviscid field was not very smooth (an advantage of *ASTET*) and the entire grid had to be generated at once. The learning curve for the ICEM software was much steeper than that of GRIDGEN, and a software training class is recommended. To conclude, only an inviscid grid was generated for the hypersonic vehicle using ICEM CFD.

After looking into several alternate grid generation possibilities, AeroSoft ended up using the multi-zone mesh generated with *ASTET* and GRIDGEN. This grid was used for both the engine off and engine on simulations which assumed turbulent flow and finite-rate chemistry. For the pull-up maneuver simulation, the perfect gas assumption was assumed, along with inviscid flow. Because of this, grids generated from both *ASTET* and ICEM CFD were possibilities. The ICEM CFD inviscid grid was more refined, and was therefore used for the flight maneuver simulation. So the final outcome proved all three grid generation packages to be useful. Grids from *ASTET*, GRID-

GEN, and ICEM CFD were used in the hypersonic vehicle simulations, but only *ASTET* was used for the unstructured viscous meshes.

## 0.6.2 Engine Off Simulation

After doing some preliminary calculations (see Sec. 0.5.1), the full three dimensional simulation with the engine off was ready to be performed. This calculation used the mesh generated using *ASTET* and GRIDGEN.

The simulation was done using finite-rate chemistry using the Kang & Dunn chemistry model. The Kang & Dunn model is a standard air model consisting of 17 reactions and 5 species. The 5 species are  $N_2$ ,  $O_2$ ,  $NO$ ,  $N$ , and  $O$ . For the thermodynamics model, equilibrium translation and rotation was assumed.

The turbulence model used for the simulation was the one-equation model by Spalart-Allmaras. The Spalart-Allmaras model is one of the most popular one-equation models, and performs on the same level as most two-equation models.

The engine off simulation was done in stages to gain understanding of the problem and to help identify issues that may arise. For example, the CFD computation began using first order inviscid fluxes with 2 of the 5 species. The chemistry model was frozen so no reactions took place. This allowed the flowfield to set up and be verified. Next, the viscous fluxes were turned on followed by adding in the remaining species. In this way numerical problems could be identified if any arose.

There were two numerical issues that came about with the simulation. First, the turbulence model required limiting to maintain stability. Limiting for the turbulence model is available in *GUST* due to strong shocks and expansions. And secondly, using second order inviscid fluxes resulted in numerical instability. Because of this, the inviscid fluxes were kept as first order.

The freestream and numerical conditions for the engine off simulation are given in Table 2.

For the boundary conditions, the freestream conditions were set for all the farfield boundaries except for the exit plane. For the exit the first order extrapolation condition was used, which is consistent for a supersonic flow exiting a domain. The vehicle surface was set to no-slip with either adiabatic heat transfer or a constant wall temperature. The constant wall temperature condition was needed upstream of the engine inlet to help position the shock

Table 2: Engine Off Conditions.

Freestream Mach No.	6.0
Angle of Attach	2 degrees
Freestream Temperature	57.59 K
Freestream $N_2$ density	0.061462 kg/m <sup>3</sup>
Freestream $O_2$ density	0.01726 kg/m <sup>3</sup>
Inviscid Flux	Van Leer
Inviscid Accuracy	First Order
Turbulence Model	Spalart-Allmaras

location. A shock was generated underneath the vehicle just ahead of the engine entrance. It was recommended that a constant wall temperature be set for the surfaces ahead of the nozzle inlet. In theory, this would help weaken or re-position the shock such that the flow through the engine would remain supersonic. The wall temperature was set to 400K.

The solid pressure contours on the vehicle body with Mach contour lines on the symmetry plane are shown in Figure 14. The same plot but with the view from the rear of the vehicle is shown in Figure 15. A shock is seen in front of the nozzle inlet, which was strong enough to reduce the flow from supersonic to subsonic as it entered the nozzle inlet. The angle of attack for this problem was two degrees. The engine on simulation was done at zero degree angle of attack and, as will be seen, the shock position changed such that the flow remained supersonic throughout the nozzle. Therefore, the angle of attack has a large part in the shock position and strength for this geometry.

A close up view of the step inside the engine is shown in Figure 16. In this plot the velocity vectors are shown and color contoured to the Mach number value. The flow is choked at the step and begins to expand at that point, going supersonic. The separation region is very small in front of the steps.

Solid pressure contours on the plane of symmetry are shown in Figure 17. Again the shock in front of the engine inlet is clearly visible. Also, the zonal boundary can be identified from the pressure contour lines. A small discontinuity in the pressure contours exist at the zonal boundary. This discontinuity becomes more distinct as you move further from the body.

This is due to the larger cell sizes that occur away from the vehicle body. Near the body the contours are smooth due to the clustering of grid cells.

The last three figures for the engine off simulation show the entire hypersonic vehicle with surface pressure contours. The entire vehicle is shown by assuming vehicle symmetry. The rear view of the vehicle is shown in Figure 18. The front view of the top and bottom of the hypersonic vehicle is shown in Figures 19 and 20 respectively. The regions of high pressure are seen mostly on the surfaces around the engine inlet. The leading edges of the wing and tail fins also reveal regions of high pressure.

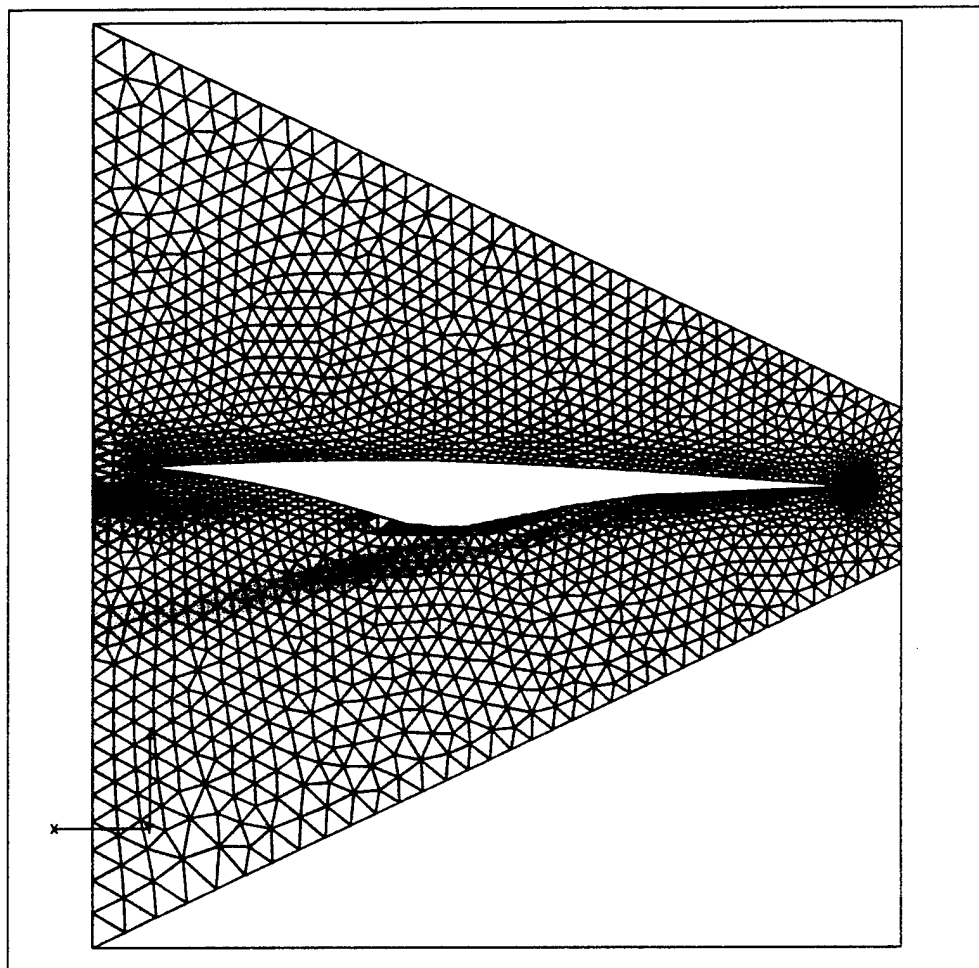


Figure 1: Pressure contours on the symmetry plane (with grid imposed) for the inviscid, three dimensional case (preliminary case 1).

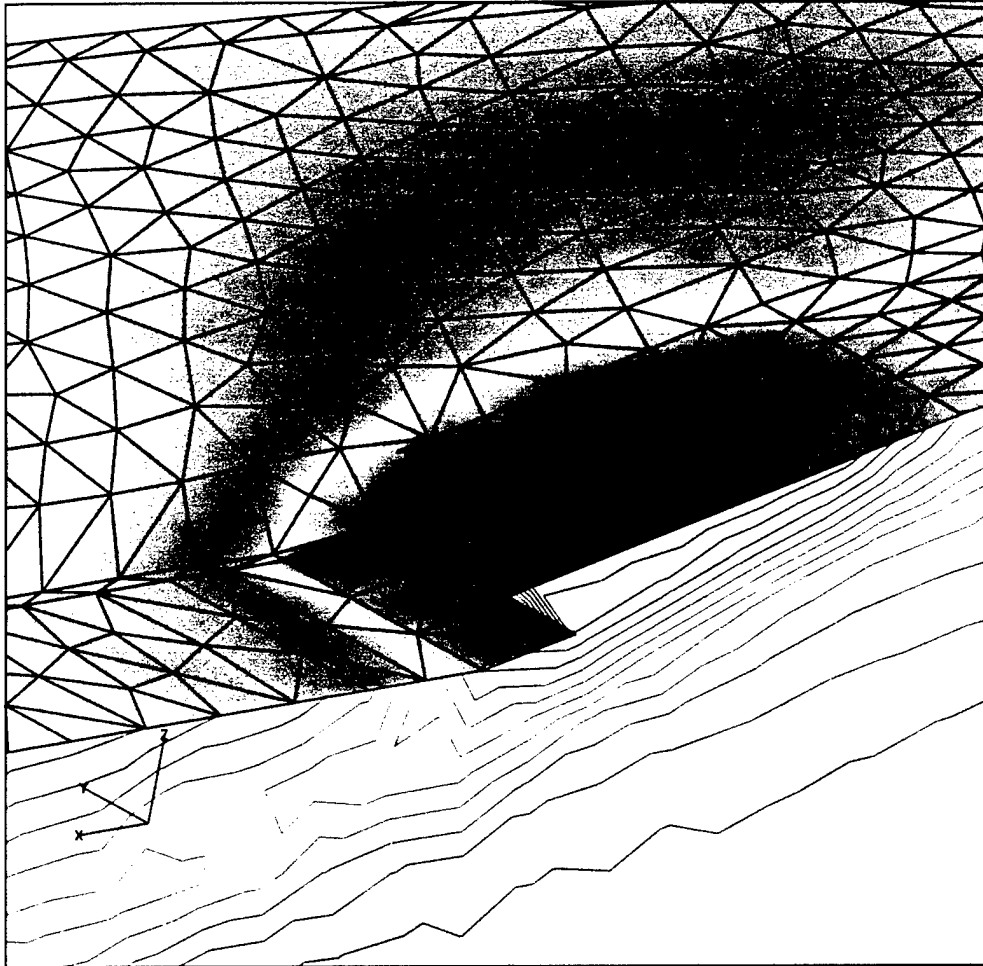


Figure 2: Surface pressure contours near the the nozzle inlet area for the inviscid, three dimensional case (preliminary case 1).

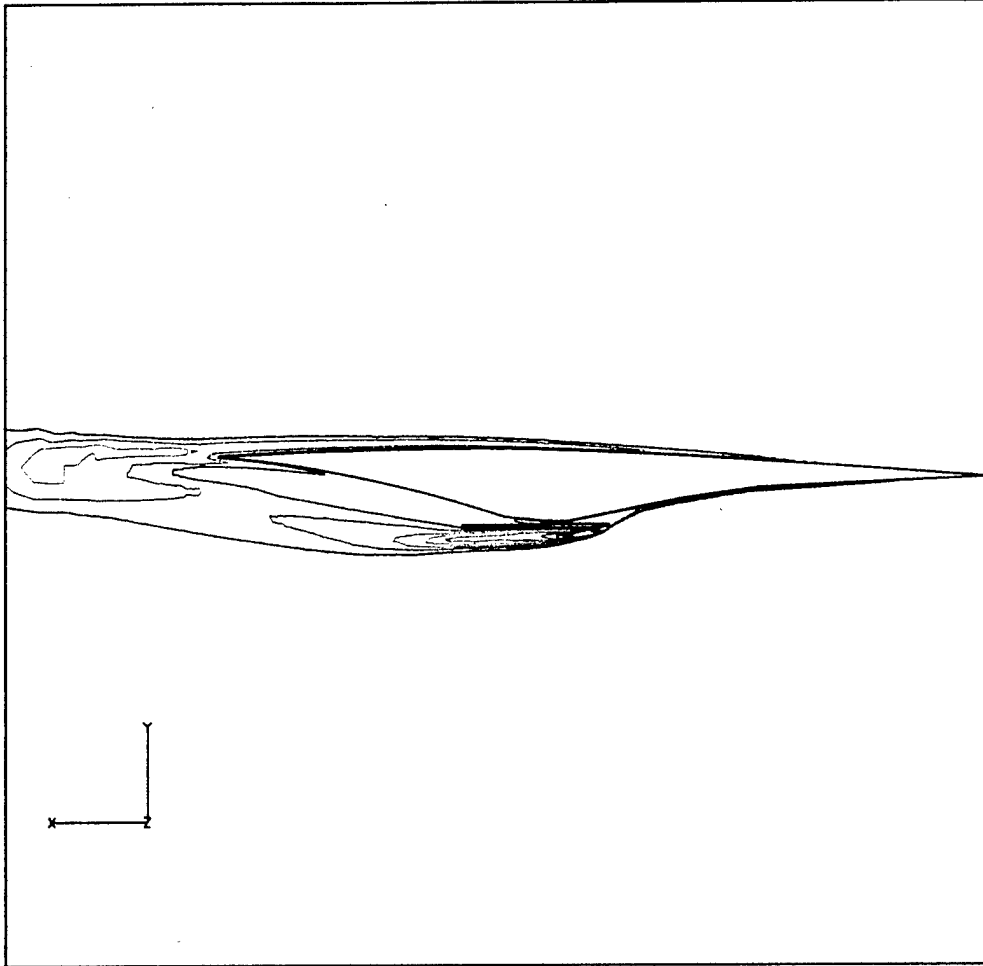


Figure 3: Contours lines showing regions where the turbulent viscosity was largest in preliminary case 2.

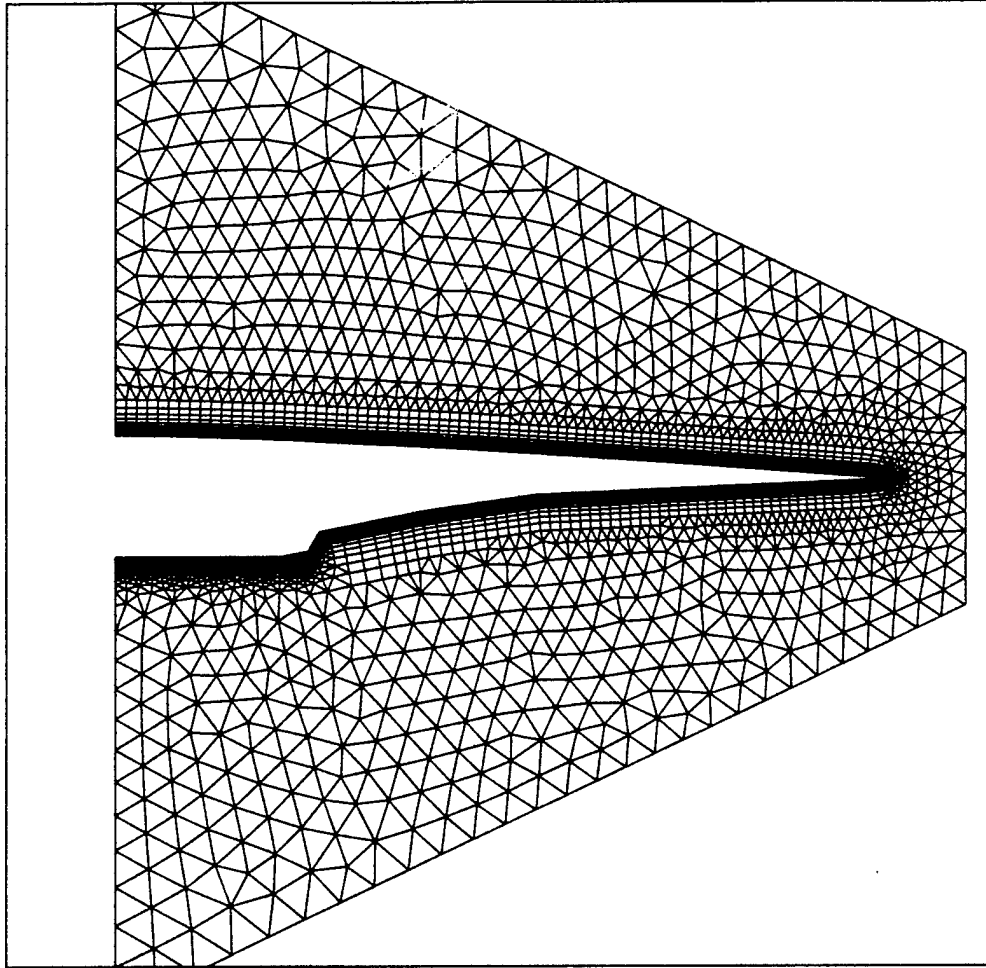


Figure 4: Grid along the symmetry plane for the 3-D viscous problem (preliminary case 3).

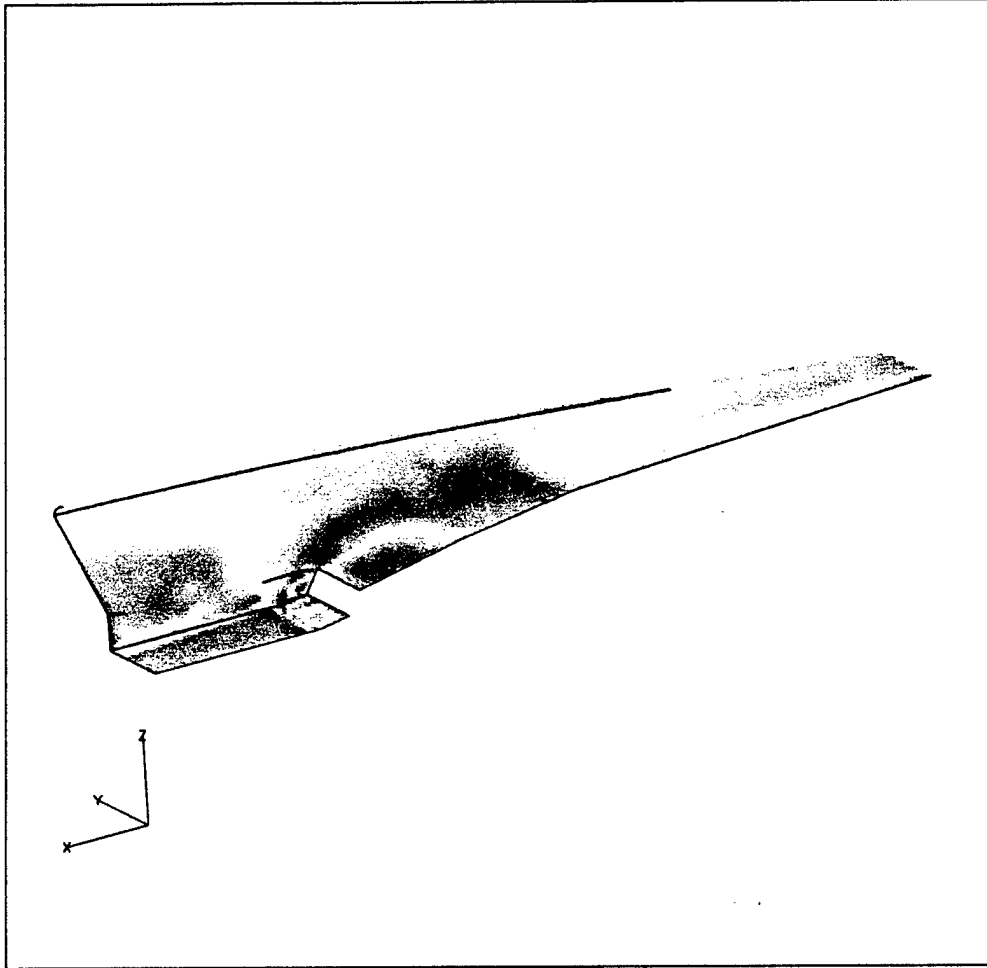


Figure 5: Pressure contours on the surface of the vehicle for the 3-D viscous problem (preliminary case 3).

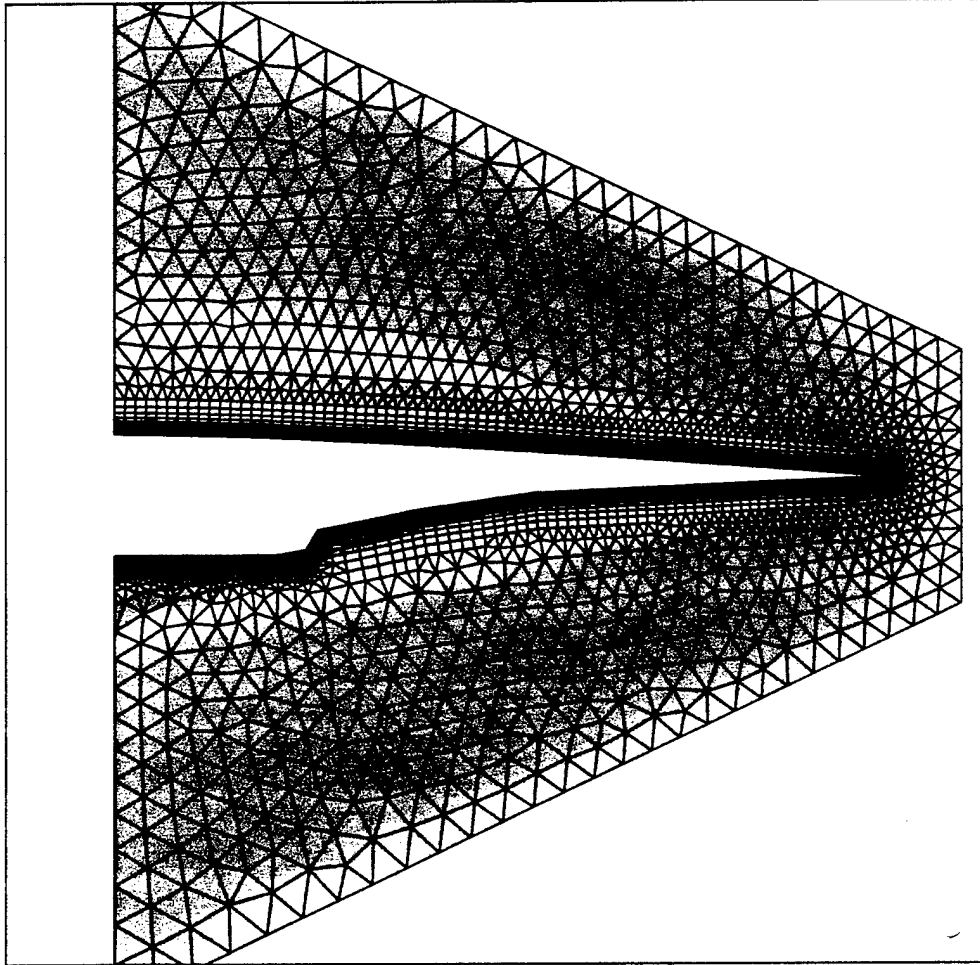


Figure 6: Pressure contours on the symmetry plane for preliminary case 3 with the grid imposed.

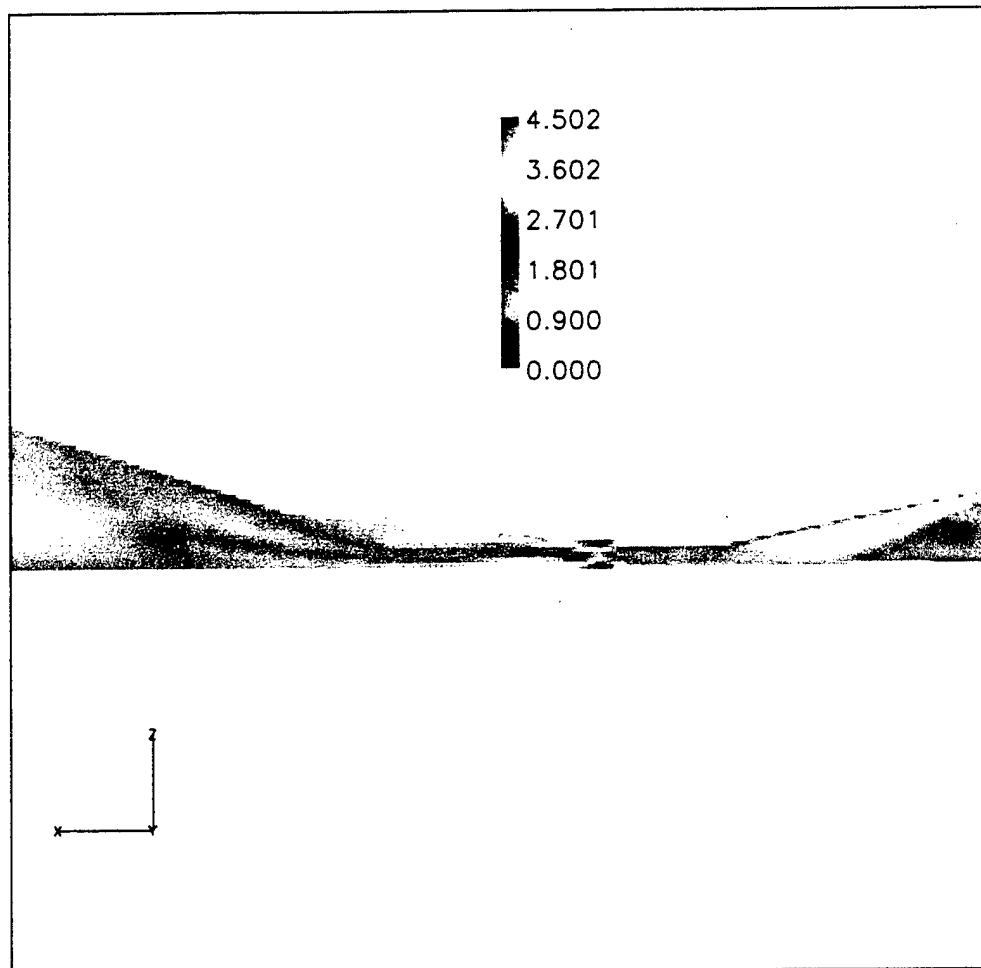


Figure 7: Mach contours inside the scramjet with combustion of hydrogen (preliminary case 4).

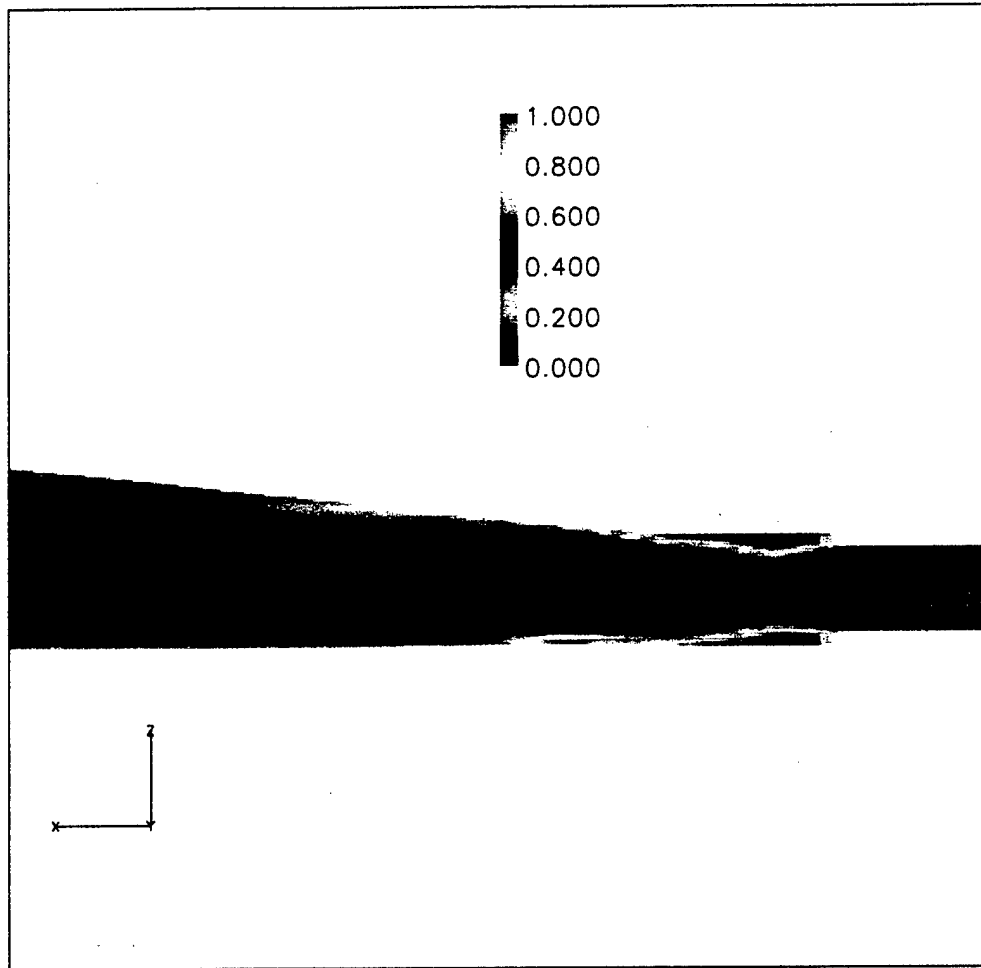


Figure 8: Contours of mass fraction for hydrogen inside the scramjet (preliminary case 4).

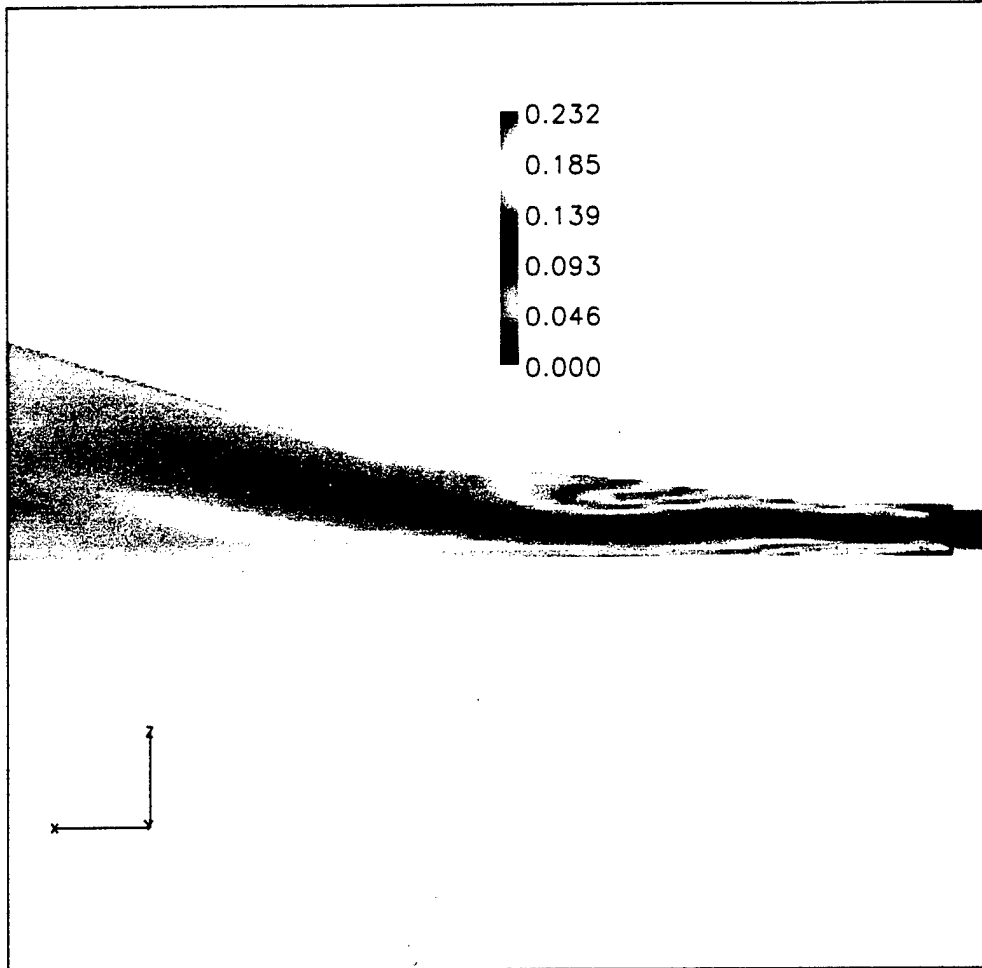


Figure 9: Contours of mass fraction for water inside the scramjet due to the combustion of hydrogen (preliminary case 4).

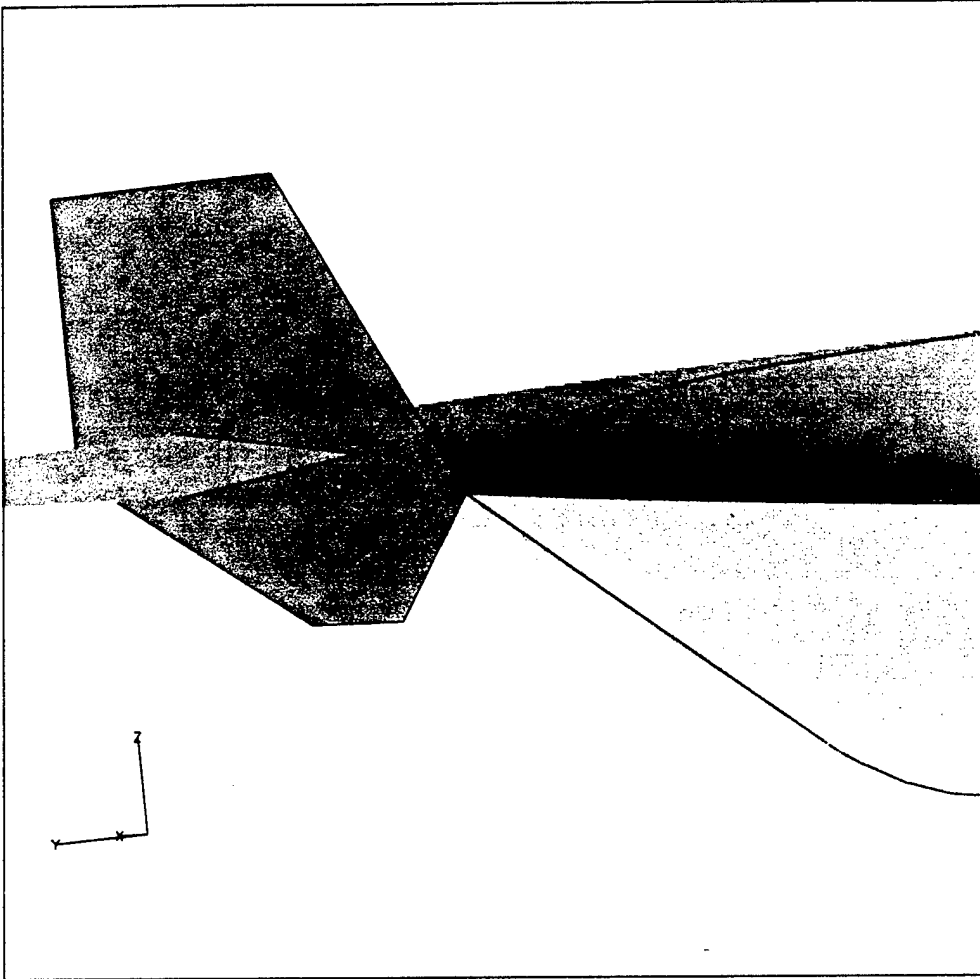


Figure 10: The hypersonic vehicle geometry where a singular point exists at the forward fin/body junction.

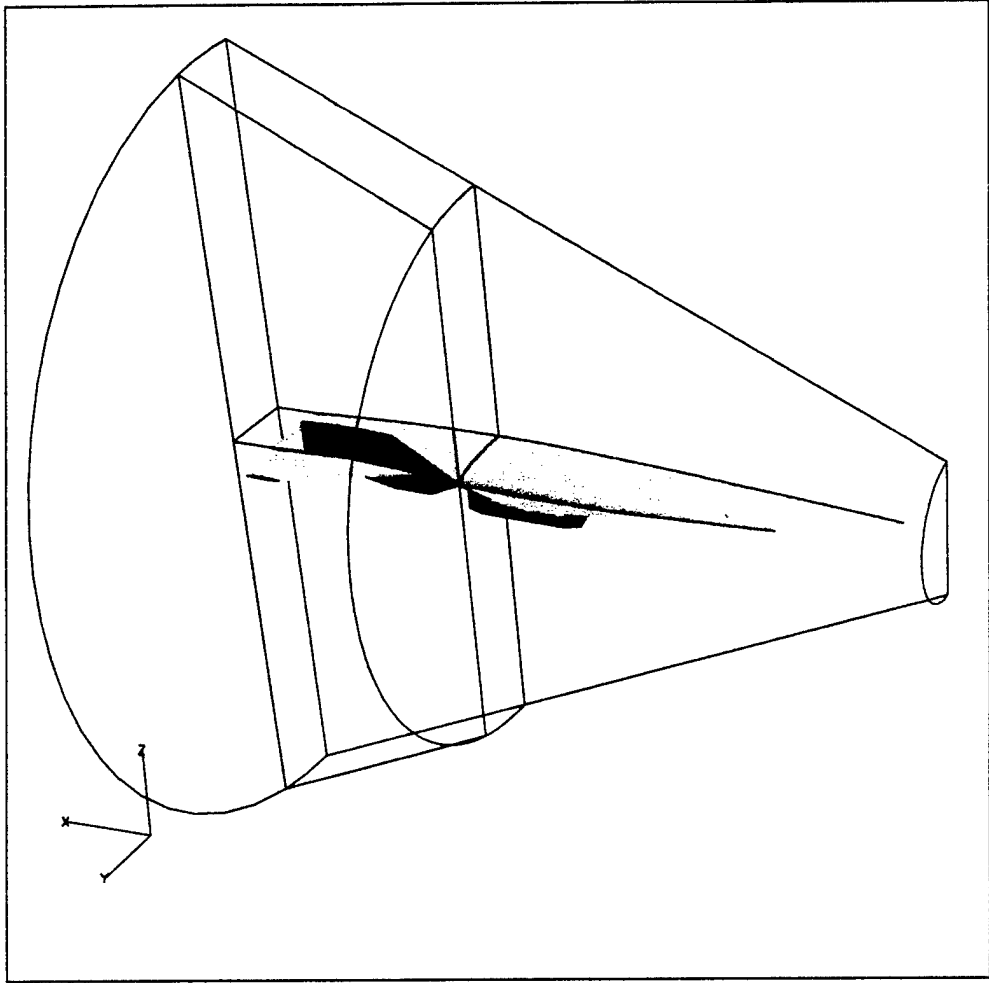


Figure 11: The hypersonic vehicle with the outline of the four *ASTET* generated zones.

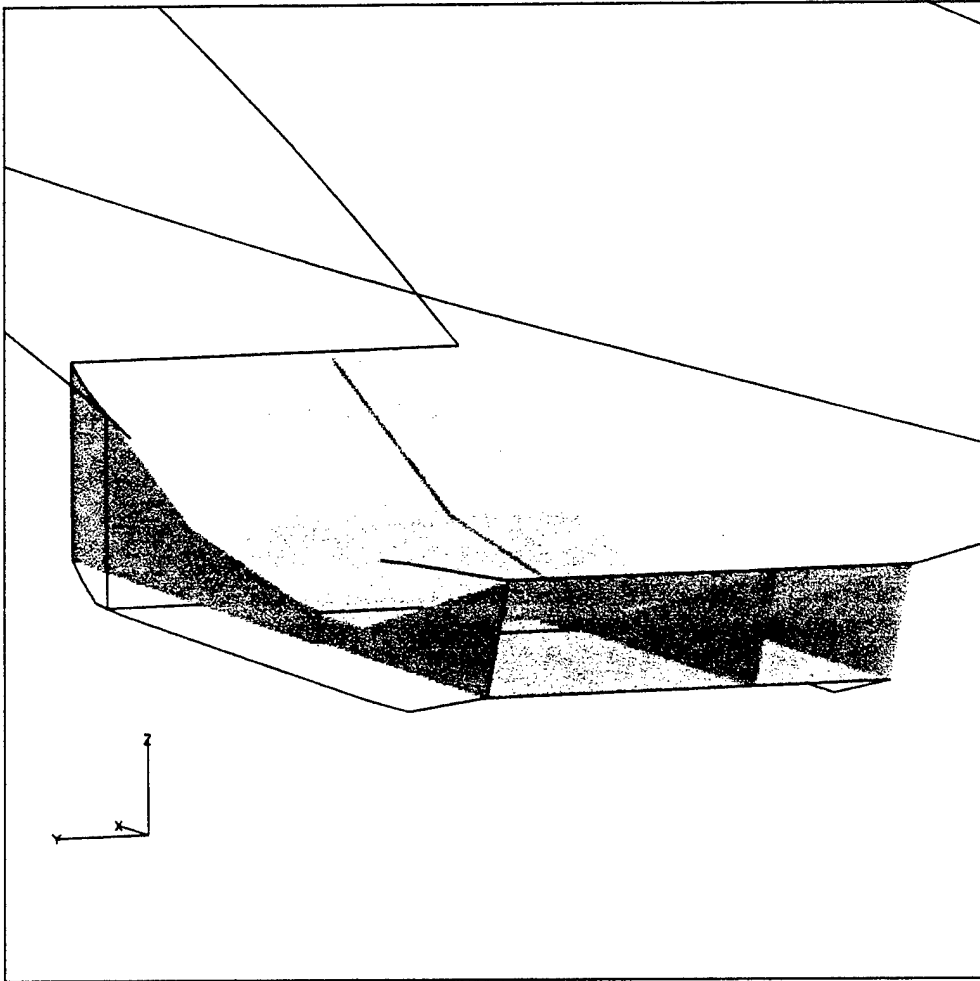


Figure 12: The internal dust (scramjet) of the hypersonic vehicle with outline of the external vehicle body. Only half of the geometry is shown due to symmetry.

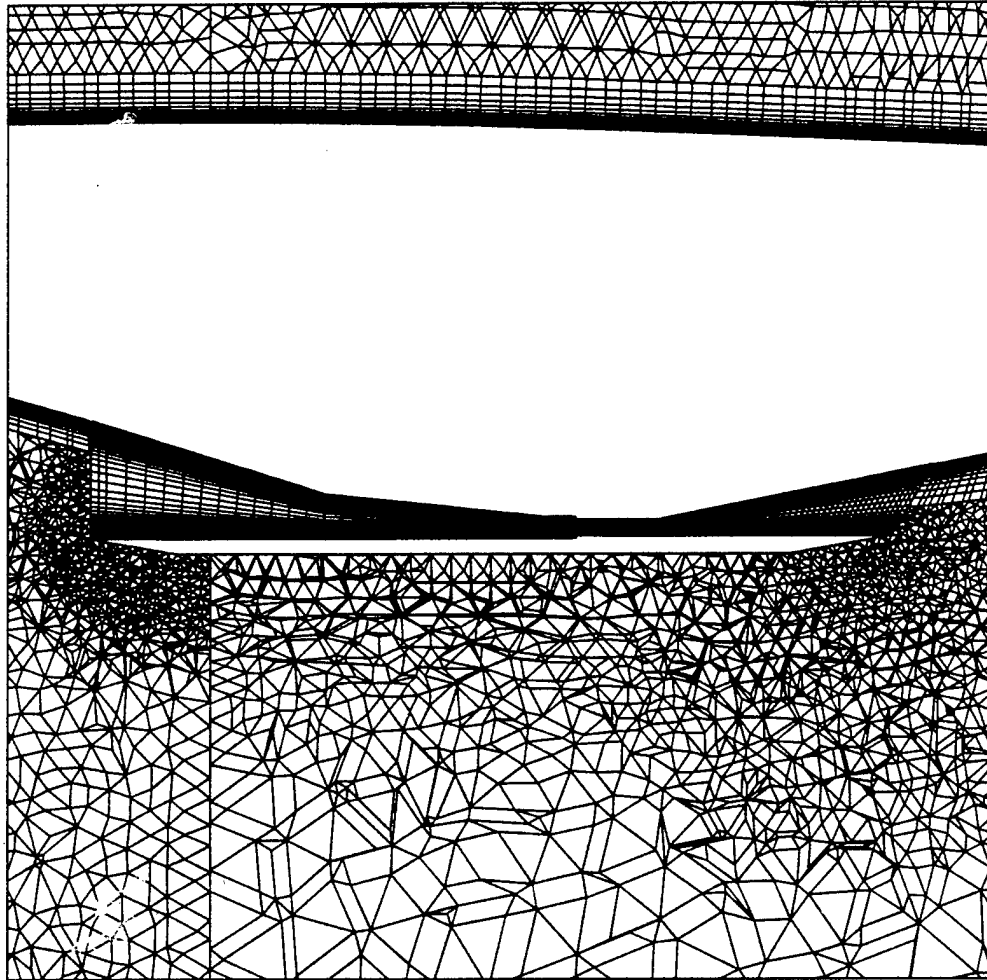


Figure 13: A slice of the hypersonic grid showing the internal duct and exterior grids.

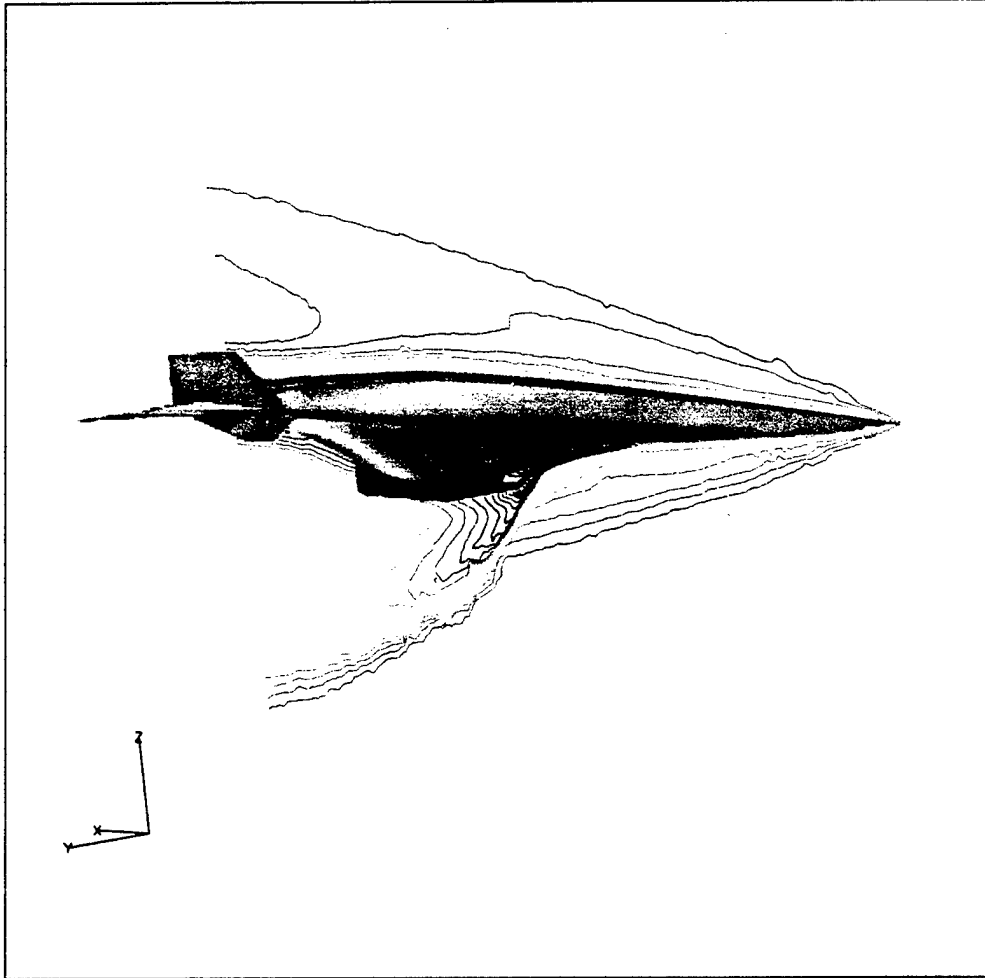


Figure 14: Solid pressure contours on vehicle body and Mach contour lines on the symmetry plane (front view; engine off).

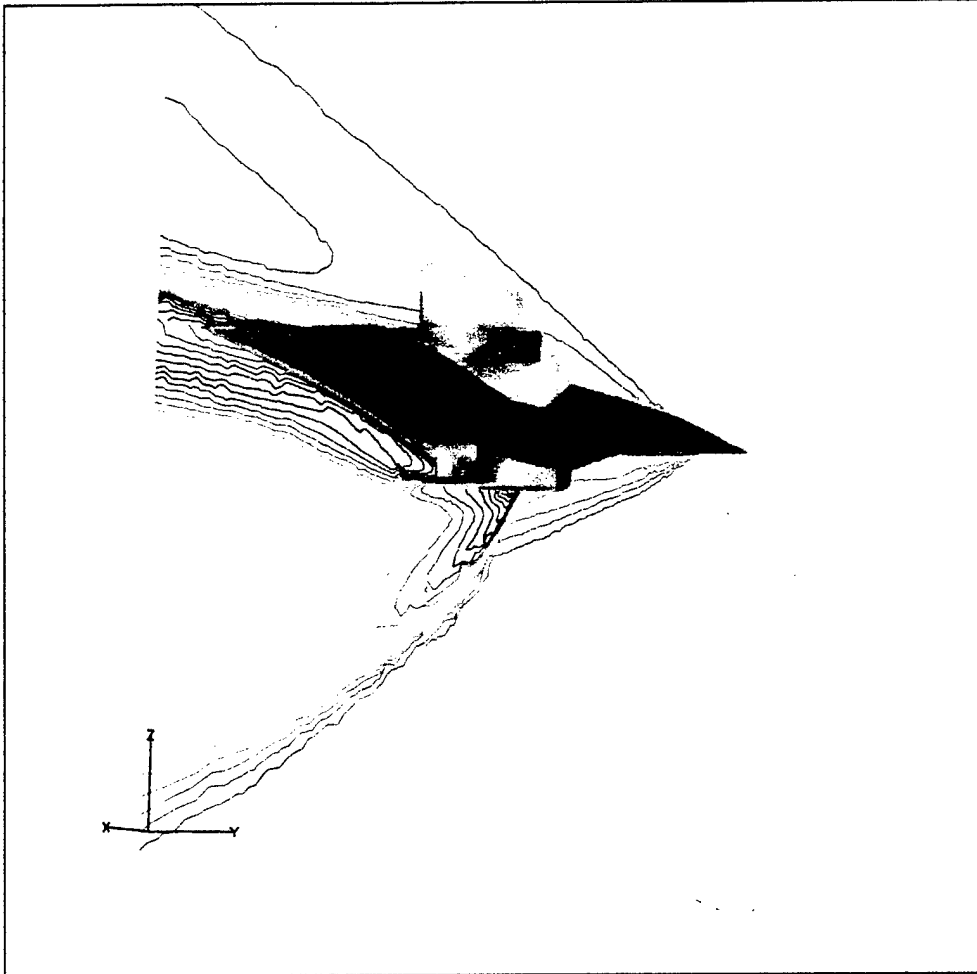


Figure 15: Solid pressure contours on vehicle body and Mach contour lines on the symmetry plane (rear view; engine off).

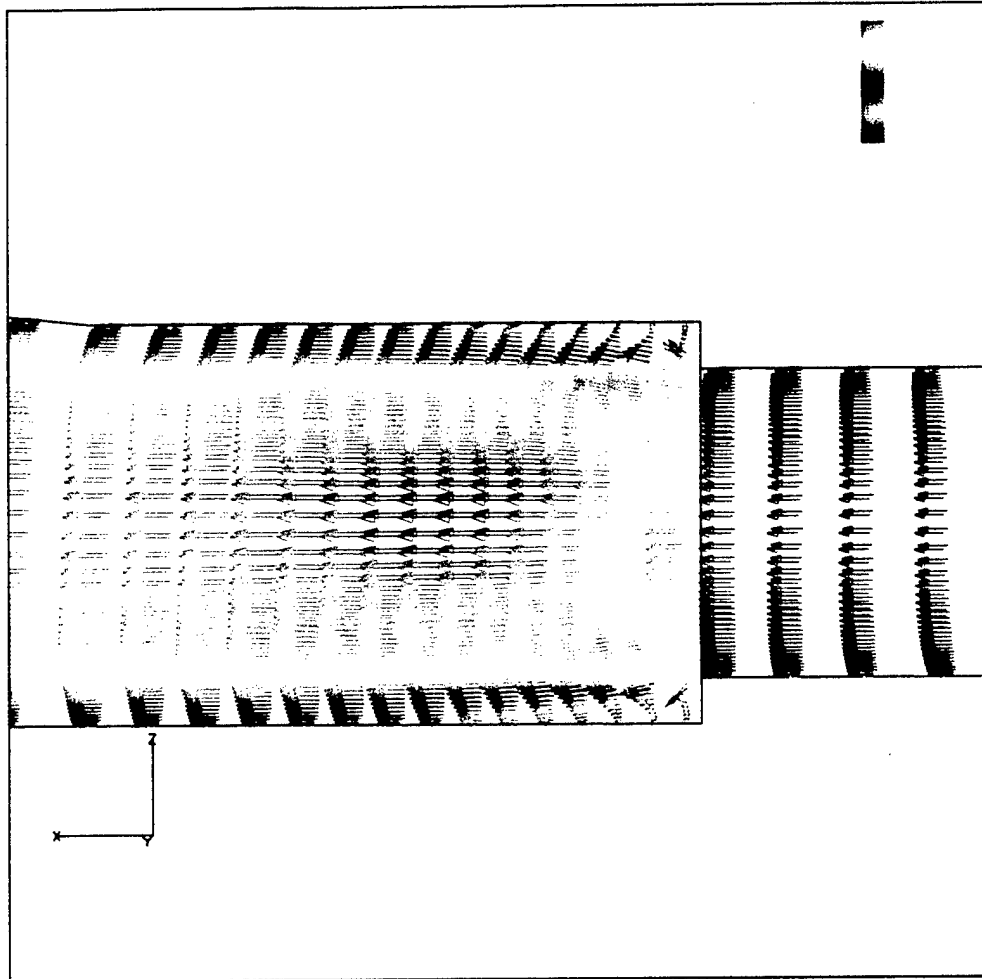


Figure 16: Up close view of the step inside the engine. Velocity vectors with color Mach number shown on the symmetry plane. Engine off.

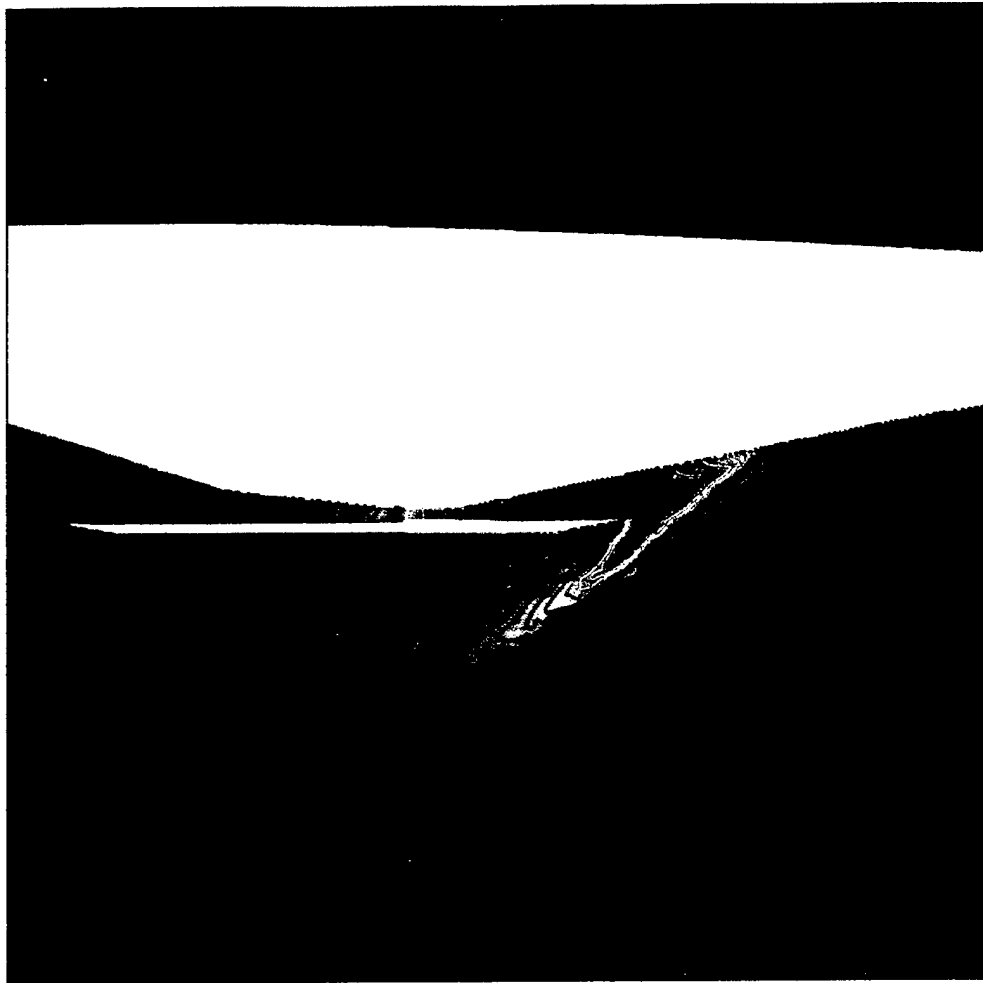


Figure 17: Pressure contours on the plane of symmetry (engine off).

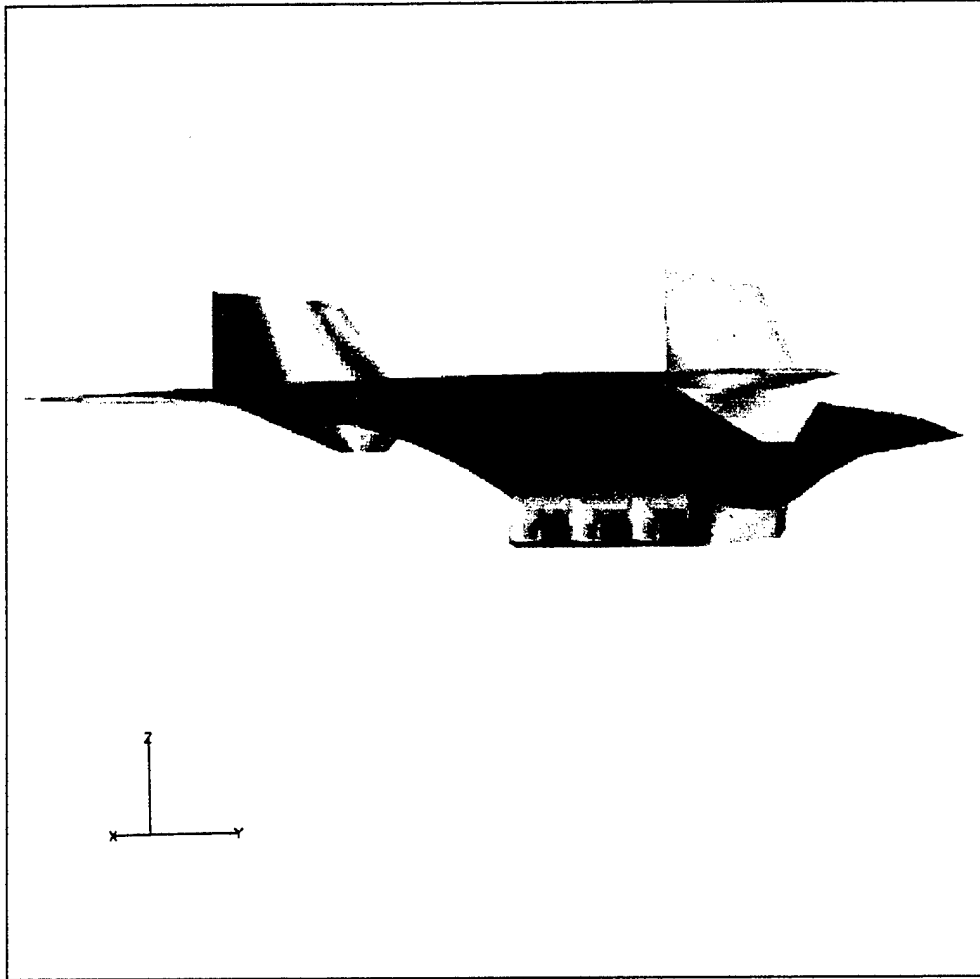


Figure 18: Surface pressure contours on the entire hypersonic vehicle body (rear view ;engine off).

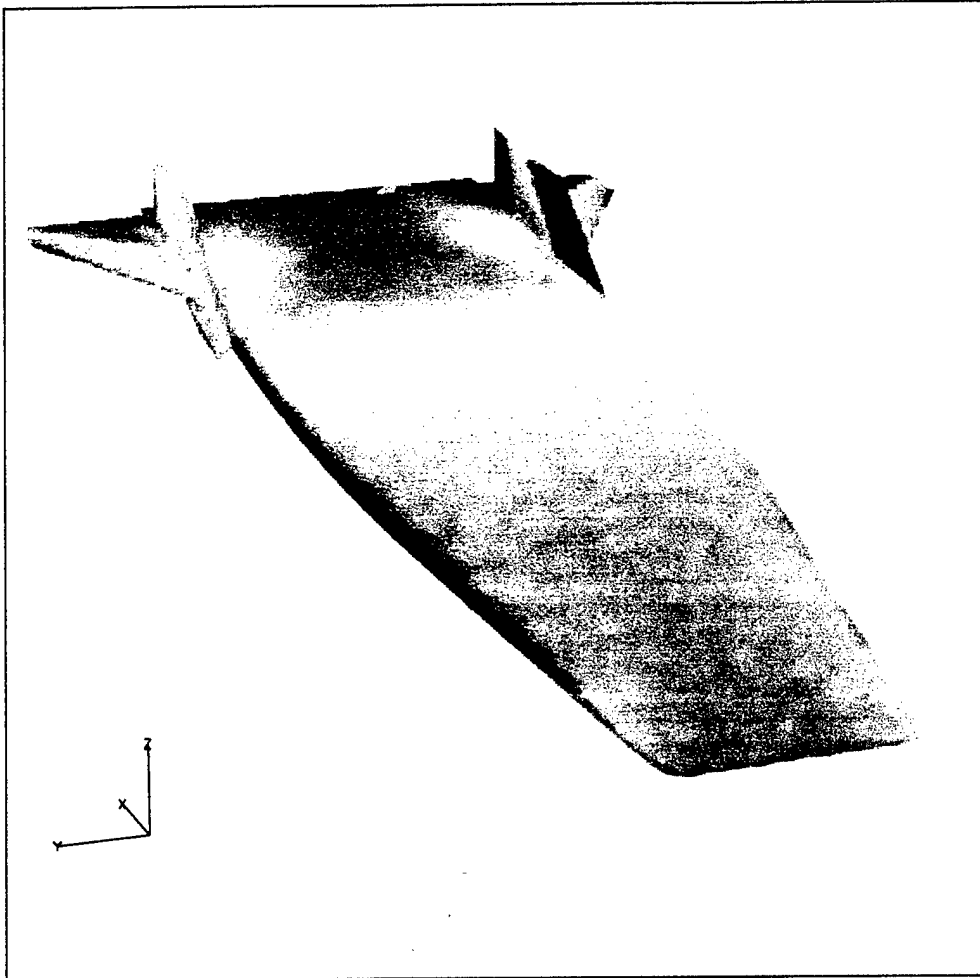


Figure 19: Surface pressure contours on the entire hypersonic vehicle body (top view; engine off).

### 0.6.3 Engine On Simulation

The engine on simulation is now discussed. Here the engine is assumed to be turned on which is modeled by injecting hydrogen into the flow. Starting with the engine off problem, there were several changes that had to be made in order to do the engine on simulation. These were: selecting a new chemistry model, changing the boundary conditions inside the engine, and setting new freestream parameters. The grid for the engine on and engine off simulations were the same.

The engine simulation is similar to a scramjet in that fuel is injected into the flow and combusts due to the presence of a flame. The combustion adds energy to the flow which causes the flow to accelerate. The accelerated flow then generates thrust.

In the present simulation, hydrogen is used as the fuel. The combustion (which is normally caused by a flame) is done by injecting the hydrogen at a high temperature (2000 K). Recall that the engine combustion was tested back in Sec. 0.5.4.

Where the engine off calculation used the Kang & Dunn air chemistry model, the engine on simulation needed an hydrogen-air chemistry model. The Drummond 1 hydrogen-air chemistry model was selected for this simulation. The model has 7 reactions and 7 species. The species are:  $N_2$ ,  $O_2$ ,  $H_2$ ,  $OH$ ,  $H_2O$ ,  $O$ , and  $H$ .

The inviscid flux used was Roe and the turbulence model was the one-equation Spalart-Allmaras model. Both the viscous and inviscid fluxes were locally second order accurate.

The freestream and numerical conditions for the engine on simulation are given in Table 3. The flow conditions are almost identical to the engine off simulation except for the angle of attack. The zero degree angle of attack was used to achieve supersonic flow throughout the engine.

Except for the hydrogen injection, the boundary conditions for the engine on simulation were identical to the ones used for the engine off computation. The hydrogen was injected into the flow along the upper and lower steps inside the engine. The steps allow the hydrogen to be mixed with the engine flow.

For the engine on simulation, two different densities were used for the hydrogen injection. The Mach number and temperature were held constant for each of the densities tested. So the higher the density value, the more hydrogen mass was being injected. A view of the step region inside the

Table 3: Engine On Conditions.

Freestream Mach No.	6.0
Angle of Attach	0 degrees
Freestream Temperature	57.59 K
Freestream $N_2$ density	0.061462 $kg/m^3$
Freestream $O_2$ density	0.01726 $kg/m^3$
Injected $H_2$ density	0.003 & 0.006 $kg/m^3$
Injected $H_2$ Temperature	2000 K
Injected $H_2$ Mach	1.05
Inviscid Flux	Roe
Inviscid Accuracy	Second Order
Turbulence Model	Spalart-Allmaras

engine is shown in Figures 21 and 22 for densities of 0.03  $kg/m^3$  and 0.06  $kg/m^3$  respectively. In both cases the flow remains supersonic at the injection site, but as the hydrogen density increases, the region of supersonic flow decreases. If the density of hydrogen were much higher, the flow would be forced to a subsonic velocity due to the mixing of hydrogen with the flow. A supersonic flow throughout the nozzle was sought after, so the density of injected hydrogen was never increased above the 0.06  $kg/m^3$  value.

The mass fractions of hydrogen and water are shown in Figures 23 and 24. The hydrogen ( $H_2$ ) is shown in Figure 23 for the injected value of 0.06  $kg/m^3$ . From the figure, the hydrogen completely combusts since there is negligible amounts of hydrogen downstream of the injection site. One of the products of hydrogen combustion is water ( $H_2O$ ). The concentration of water (mass fraction) is shown in Figure 24 for the 0.06  $kg/m^3$  hydrogen injection case. The water remains near the wall and slowly mixes with the other species as the flow moves toward the engine exit.

The Mach contours for the entire symmetry plane is shown in Figure 25. For the freestream conditions stated above and with hydrogen being injected at a density of 0.06  $kg/m^3$ , the Mach number exiting the engine is below the freestream value of 6. In order for a positive thrust force to be achieved, the flow would need to be accelerated to speeds greater than the freestream flow.

Since AeroSoft was not given engine conditions for the combustion process, it would be difficult to setup the injection conditions needed for positive

thrust generation. It is clear that more hydrogen injection is necessary, but as stated above this would cause the flow to slow to subsonic speeds. AeroSoft demonstrated engine combustion for two different injection values, thus fulfilling the objective for an engine on simulation.

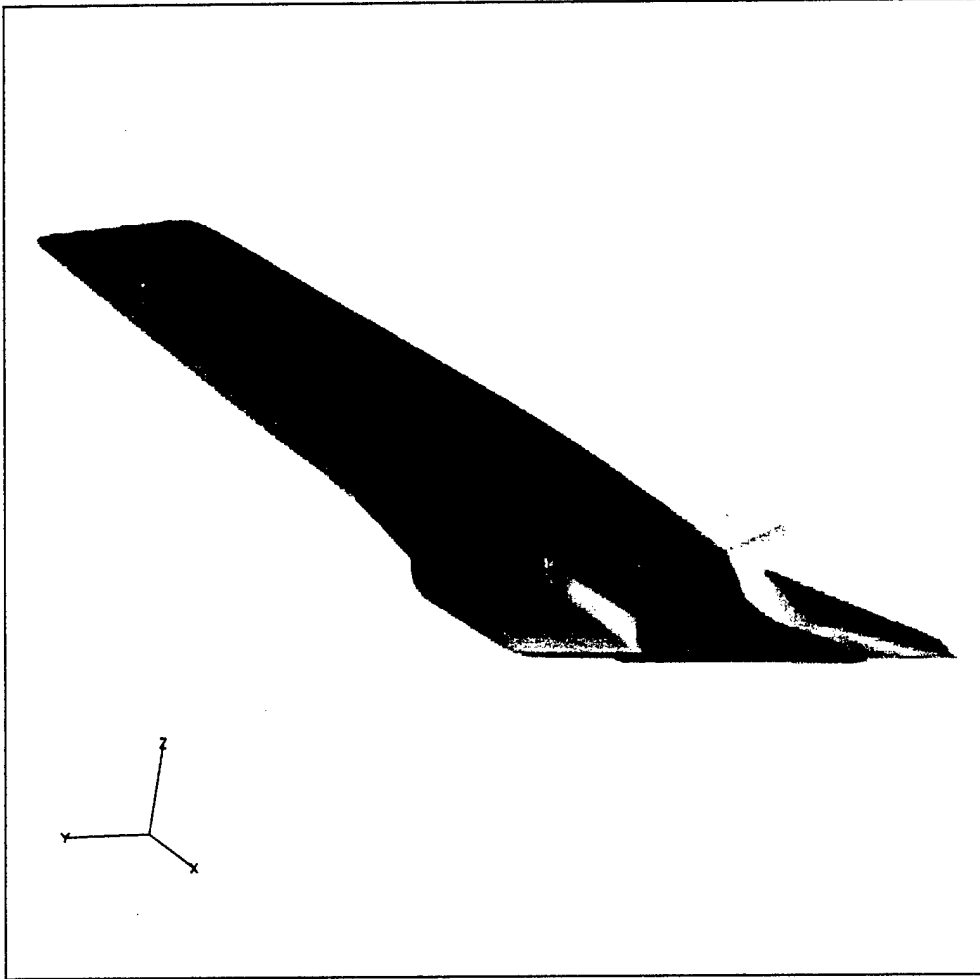


Figure 20: Surface pressure contours on the entire hypersonic vehicle body (bottom view; engine off).

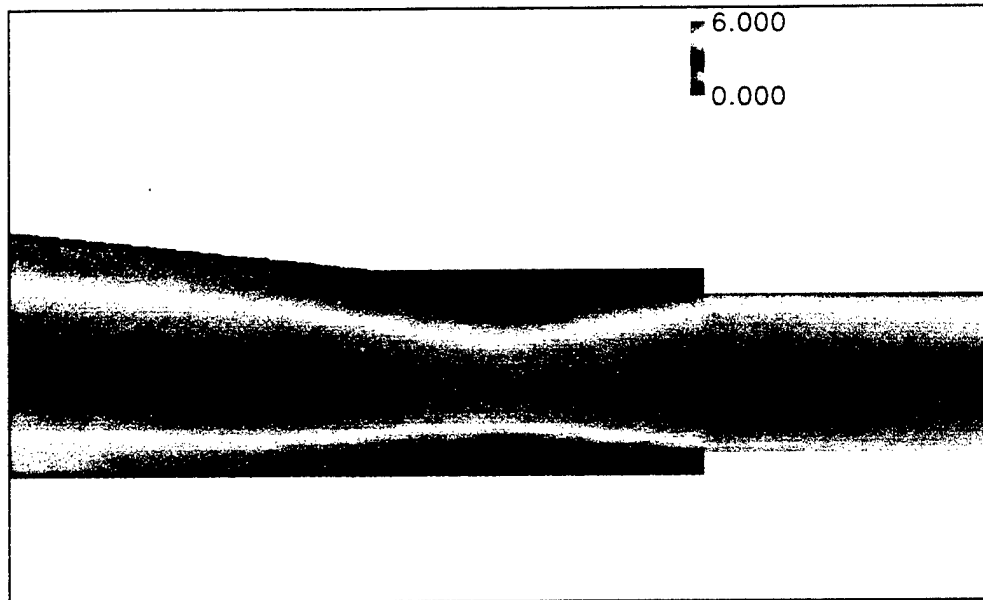


Figure 21: Step region inside engine where hydrogen is injected with a density of  $0.03 \text{ kg/m}^3$  (engine on).

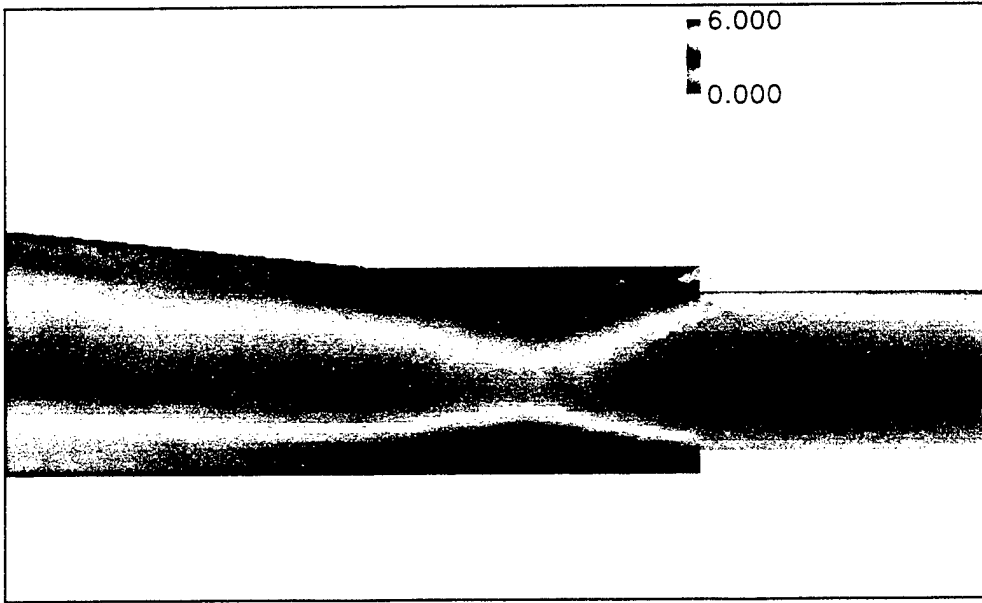


Figure 22: Step region inside engine where hydrogen is injected with a density of  $0.06 \text{ kg/m}^3$  (engine on).

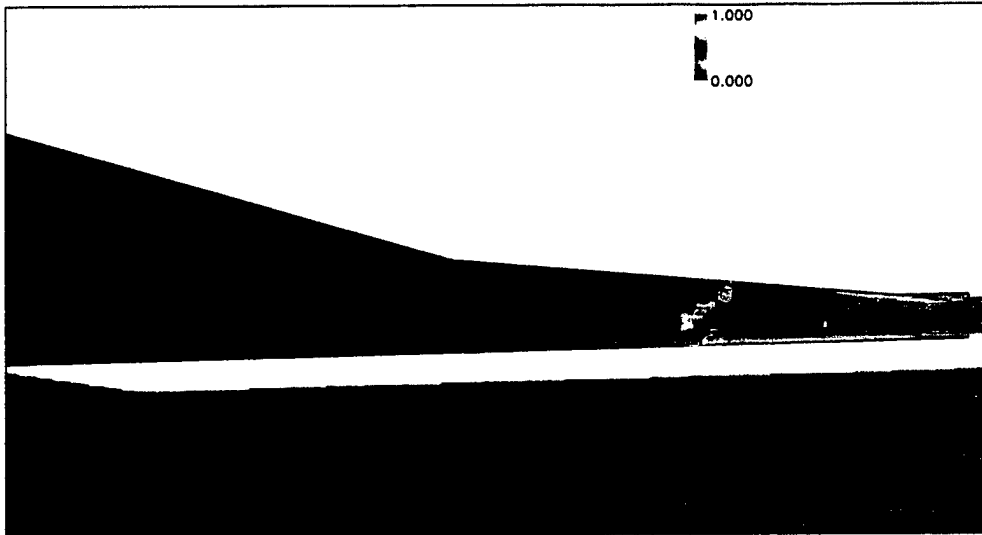


Figure 23: Mass fraction of hydrogen ( $H_2$ ) inside the engine. Contours shown on symmetry plane with injected hydrogen density of  $0.06 \text{ kg/m}^3$ .

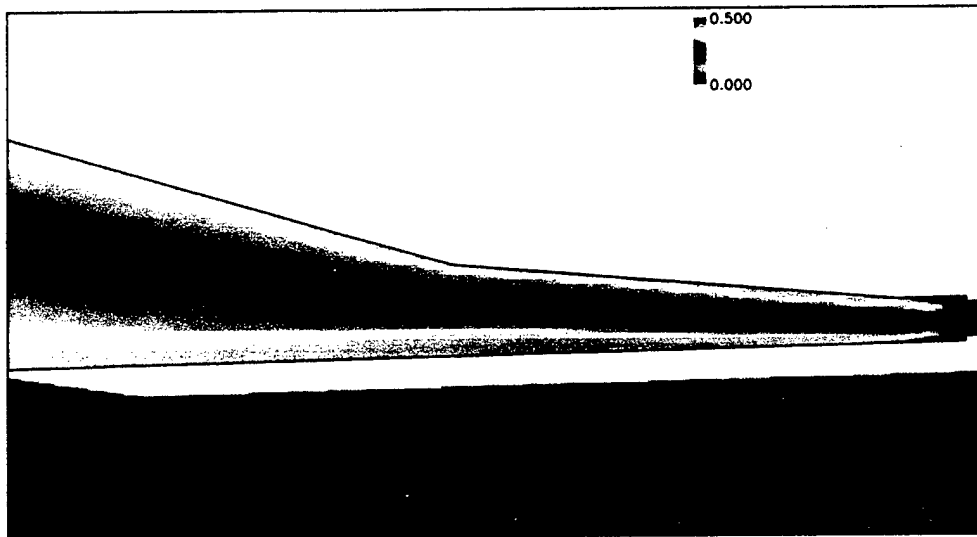


Figure 24: Mass fraction of water ( $H_2O$ ) inside the engine. Contours shown on symmetry plane with injected hydrogen density of  $0.06 \text{ kg/m}^3$ .

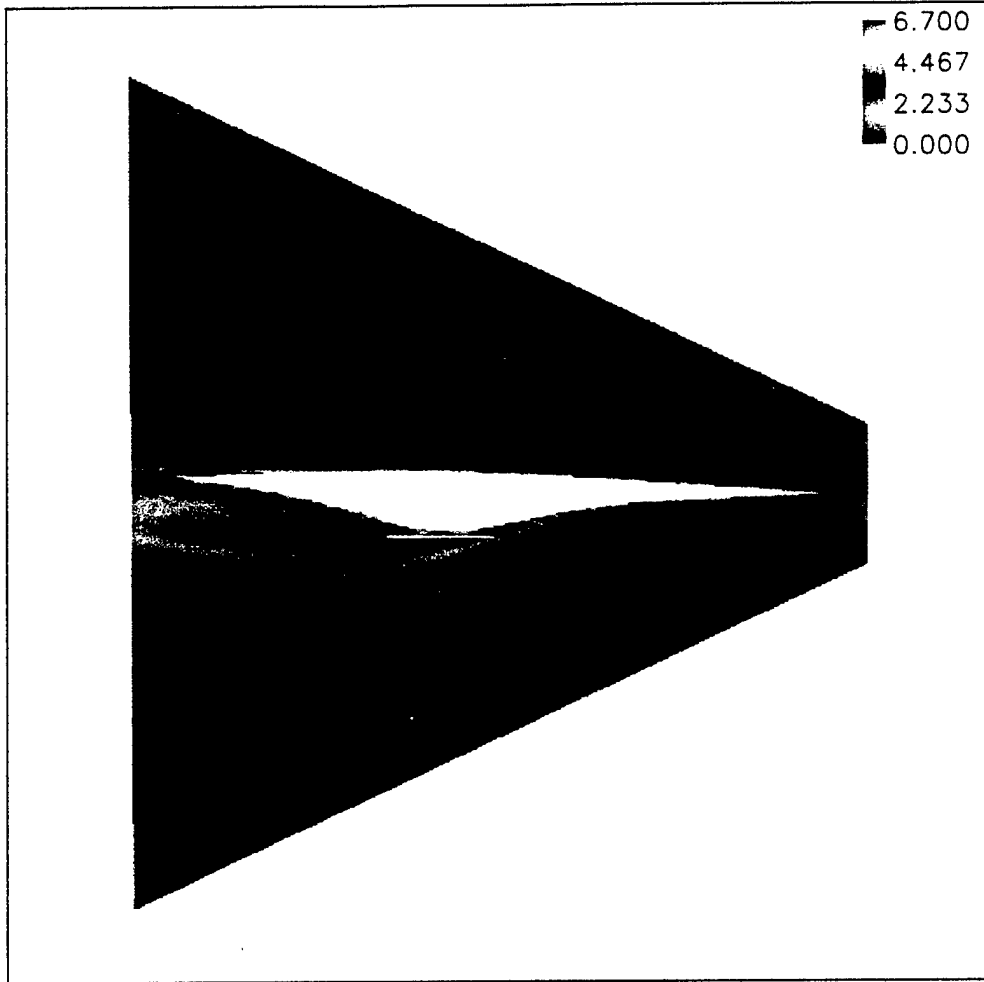


Figure 25: Solid Mach contours on the symmetry plane for the engine on simulation (injected hydrogen density of  $0.06 \text{ kg/m}^3$ ).

#### 0.6.4 Time Accurate Simulation

After performing the engine off and engine on simulations, the time accurate calculation was done. This was the last objective to be performed. This CFD simulation modeled a pull-up maneuver for the hypersonic vehicle.

The maneuver performed was a 2.5g pull-up at Mach 6. In a pull-up maneuver, the pilot increases the angle of attack causing the flight path to curve upwards. If done quickly, the velocity of the aircraft will not immediately decrease and the flight path will follow an arc with a constant radius. The computation performed here will simulate the initial stage of a pull-up where the velocity is assumed constant and the flight path follows an arc of constant radius.

In the actual 2.5g pull-up maneuver, the load on the aircraft will increase until it reaches the 2.5g target, at which time it will maintain a constant loading. The velocity will eventually begin to decrease and the flow direction will change to maintain the 2.5g loading. In the *GUST* calculation performed here, the flow speed and direction will remain constant, which is a valid assumption for the beginning stages of a quick pull-up maneuver.

Using basic aircraft performance theory, the pull-up rate and radius can be determined for a 2.5g maneuver at Mach 6. With the rotation rate and arc radius, the flight path can also be determined. *GUST* will perform the pull-up maneuver by rotating and translating the grid each time step based on the flight path and rotation rate. This is the method that *GUST* uses to perform moving body maneuvers. The grid is moved (rotation and translation) each time step, creating time metrics which will take into account the motion.

It is assumed that the aircraft is in steady flight at zero degree angle of attack when the maneuver begins. So in a way, the aircraft is positioned at the bottom of a circle and will begin to follow the path of an arc. The distance traveled in the vertical direction will be small at first, but will increase as time progresses. The rate of rotation is constant, so the aircraft will rotate by the same amount each time step. The details for the pull-up maneuver are listed in Table 4.

*GUST* solves time accurate problems using the method of dual time stepping. In this method, a time step is iterated upon until either the convergence is met or a set number of cycles are performed. The time accuracy can be either first, second, or third order. *GUST* stores the solution from the previous two time steps in order to do higher order time accuracy.

When running a time accurate moving body problem, the user can store

Table 4: Pull-Up Information.

Load	2.5g
Rotation Rate	1.54 <i>deg/sec</i>
Radius of arc	56,590 <i>m</i>
Mach	6
Temperature	57.59 <i>K</i>
Density	0.078722 <i>kg/m<sup>3</sup></i>

solutions at specified time steps. This allows the user to go back and post-process data for any time level that was saved. When saving the solution, *GUST* saves both the solution variables and the grid at that time level. In this way the user has the grid position saved as well. The numerical data for the time accurate pull-up maneuver is listed in Table 5.

Table 5: Pull-Up Information.

Time Accuracy	First
Time Step	0.01 <i>sec</i>
Save Intervals	0.1 <i>sec</i>
Inner Iterations	50
CFL	0.2

For the time accurate computation, a single zone grid was used. The grid was generated using the ICEM CFD grid generation software package. The grid consisted of 791,018 tetrahedral cells. The grid was symmetric about the hypersonic vehicle such that only half of the vehicle was simulated. This prevents a simulation that involves yaw, but allows for a more efficient simulation for the pull-up maneuver.

The computation was done assuming and inviscid, perfect gas flow. A steady state solution was first solved for on the grid at Mach 6 and zero degree angle of attack. The forces were monitored to assure convergence. Once the steady state flow was attained, the problem was restarted in time accurate mode. The solution was saved every 0.10 seconds and the forces were printed out every time step (0.01 seconds).

The force history for the pull-up maneuver is displayed in Figure 26.

The vertical force ( $z$  direction) was fairly constant at first and then began increasing at a linear rate. The axial force ( $x$ ) also increased linearly while the side force ( $y$ ) stayed fairly constant. The 2.5 load factor was reached after 1.32 seconds. The time accurate simulation was stopped at 1.34 seconds.

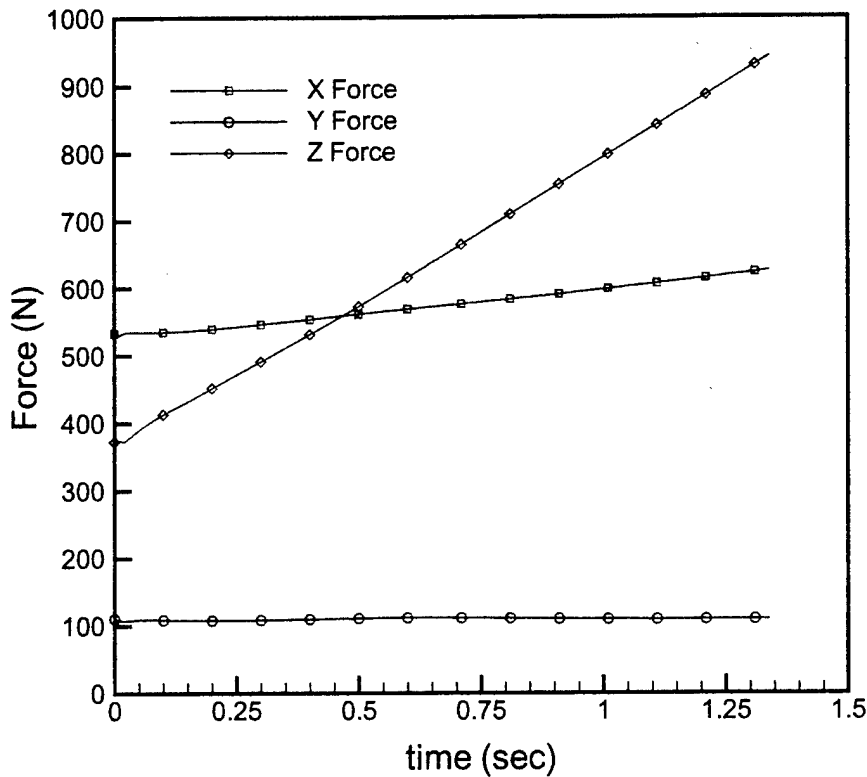


Figure 26: The force history for the pull-up maneuver. The 2.5g mark was reached at time 1.32 seconds.

At the end of the simulation (1.34 seconds), the hypersonic vehicle had rotated 2.06 degrees and traveled over 12 meters vertically. A view of the hypersonic vehicle at various times throughout the pull-up maneuver are shown in Figure 27. The figure is to scale for the relative positions of the vehicle, but note that the forward motion of the vehicle over the 1.34 seconds

is not reflected in the figure. The bottom vehicle is at time 0 seconds, the other times correspond to 0.91 and 1.31 seconds (as vertical position increases respectively).

## 0.7 Conclusions

The objectives of this contract were to perform three CFD simulations for a hypersonic vehicle. The CFD code used to perform the simulations was *GUST*, AeroSoft's unstructured Navier-Stokes flow solver. The simulations included real gas effects and turbulence modeling.

The three simulations for the hypersonic vehicle included two steady state calculations and one prescribed motion. The steady state simulations were performed at Mach 6 with both engine on and engine off conditions. The engine on simulation modeled the combustion of hydrogen. The maneuvering flight simulation was a 2.5g pull up where the vehicle underwent both rotation and translation.

As a first step to accomplish the three simulations, several preliminary calculations were performed. These calculations were simplifications of the full problem. This was done to gain a better understanding of the physics and numerics which would later be used in solving the full simulation cases.

Once the preliminary calculations were performed, the engine off simulation was accomplished. An air chemistry model was used along with a one-equation turbulence model. Following this was the engine on simulation, which used a hydrogen-air chemistry model and again the one-equation turbulence model. Two different conditions for the hydrogen injection were performed for the engine on simulation.

And to complete the objectives, a 2.5g pull up maneuver for the hypersonic vehicle was done. This simulation was performed assuming perfect gas and inviscid flow.

One of the issues that arose from these simulations was unstructured grid generation and mesh quality. The complex geometry of the hypersonic vehicle proved to be a challenge for mesh generation. Along with AeroSoft's own grid generation package (*ASTET*), two other commercial grid generation software packages were looked at. In the end, *ASTET* was used to generate an hybrid, multi-zone mesh with non point-to-point zonal boundaries for the viscous simulations. The other two grid generation packages also produced grids that were used in the simulations, but to a lesser degree. Only *ASTET*

was used to generated unstructured viscous grids.

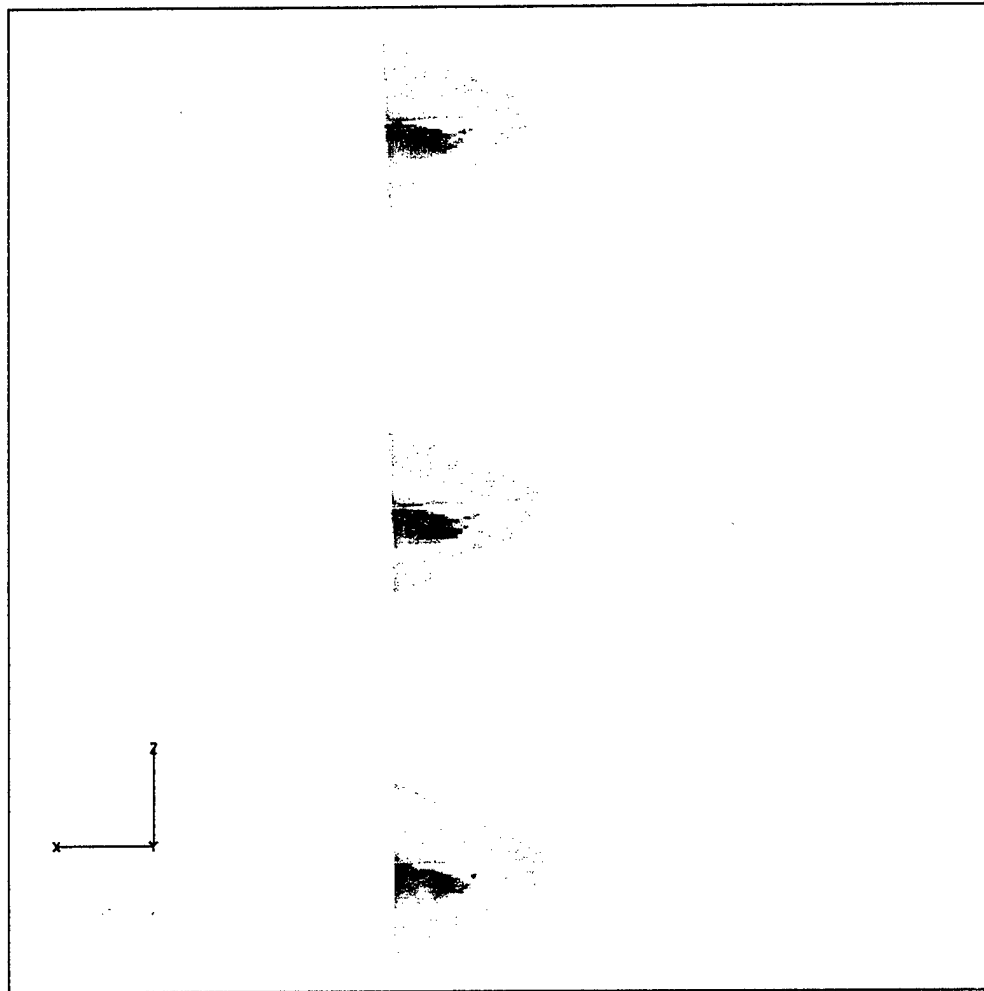


Figure 27: The hypersonic vehicle at different times during the pull-up maneuver. Symmetry Mach number contours shown.